A multi-meteorological comparison for episodes of PM_{10} concentrations in the Berlin agglomeration area in Germany with the LOTOS-EUROS CTM

M. Thürkow[1], I. Kirchner[1], R. Kranenburg[2], R. M. A. Timmermans[2] and M. Schaap[1, 2]

[1]Institute of Meteorology, Freie Universität Berlin, Carl-Heinrich-Becker-Weg 6-10, 12165 Berlin, Germany

[2]TNO, department Climate Air and Sustainability, Princetonlaan 6, 3584 CB Utrecht, the Netherlands

Corresponding author: Markus Thürkow (markus.thuerkow@met.fu-berlin.de)

Submitted to

Atmospheric Environment

July 2020

Highlights:

- An interface of the LOTOS-EUROS CTM to the COSMO-CLM model was developed
- Planetary boundary layer conditions were significantly improved by the COSMO-CLM model compared to the ECMWF reference data, but no clear bias correction was found when applying different parametrization simulations
- Higher resolved model simulations lead to a more realistic representation of the urban-increment, with the impact on the PM mass concentration of the refined vertical layering is much larger compared to the meteorological input-data
- Ammonium and Nitrate responded highly sensitive to different simulation set-ups

Abstract

Particulate matter (PM) remains as one of the most relevant air-quality concerns in urban environments. The Berlin agglomeration area is still affected by exceedances of the daily limit value of the PM concentration, especially during wintertime PM episodes. In this study, we present test-case studies with the LOTOS-EUROS CTM to improve the representation of PM episodes in the Berlin agglomeration area. A variety of simulations were compared for two winter episodes characterized by cold stagnant conditions, using different meteorological input data (from the European Centre for Medium Weather Forecast (ECMWF) and the Consortium for Small-Scale Modelling-Climate Limited-area Modelling (COSMO-CLM)) and horizontal and vertical resolutions of the LOTOS-EUROS CTM. The LOTOS-EUROS CTM indicates too high mixing from the planetary boundary layer (PBL) to higher layers, leading to an underestimation of the PM mass concentration in the Berlin agglomeration. As major impact factor the mixing-layer height (MLH) can be identified. Through applying the COSMO-CLM model the meteorological representation of the PBL and MLH can significantly be improved, whereas sensitivity studies only exhibit a small variation of the PBL meteorology and did not further improve the MLH. As the MLHs of both models are underestimated compared to observations and their derivation is questionable, we advise not to use this quantity any longer in CTMs. By contrast, applying a multi-level approach excluding the MLH, provides a considerable increase in the total PM mass concentration amount. The redistribution and increased nitrate and ammonium concentration can be mentioned as the main culprit. However, the best-fit simulations were obtained for the multi-level configuration fed by COSMO-CLM input data, additionally representing a more realistic urban increment.

Keywords: particulate matter, LOTOS-EUROS, COSMO-CLM, planetary boundary layer, composition of PM

1 Introduction

Poor air quality is one of the most important environmental concerns of the 21st century (Lim et al., 2012). Exposure to particulate matter (PM) is thought to dominate the health impacts of air pollution (Boldo et al., 2006; Brook et al., 2010; Costa et al., 2014). According to the European Environment Agency each year about 62.300 premature deaths in Germany are caused by fine particulate matter ($PM_{2.5}$) (EEA, 2018). Although a large part of the urban population in Germany is exposed to concentrations above the PM target value of the World Health Organization (WHO, 2005), the annual limit values for both $PM_{2.5}$ and PM_{10} as introduced by the European Ambient Air Quality Directive (EC, 2008) are currently not exceeded across Germany (UBA, 2019). In practice, the daily mean limit value for PM is more stringent than the annual mean limit values (Engler et al., 2012) and is still exceeded at traffic sites throughout Germany (UBA, 2019). To enable the development of cost-effective mitigation strategies to further reduce the health impacts by PM and the number of limit value exceedances it is required to understand the sources and processes leading to the enhanced concentration levels in episodes as compared to normal conditions (Belis et al., 2020).

PM concentrations are the result of processes involving direct emissions, chemical transformations, vertical mixing, long-range transport and dry and wet deposition, all depending on meteorological parameters (H. Zhang et al., 2015). Hence, establishing the origin of PM is complex as the contributions from local and distant, natural and anthropogenic, as well as individual source sectors vary largely with season and synoptic situation (Tai et al., 2010; Mues et al., 2012; H. Zhang et al., 2015). High concentrations of PM are often associated with cold and stagnating weather conditions (Tai et al., 2010). Although the exceedances of limit values occur especially at the local urban scale (van Pinxteren et al., 2019), the regional background provides the most important mass contribution to observed PM levels in European cities (Beekmann et al., 2015; Garg & Sinha, 2017). Berlin, and East Germany in general, are affected by air masses from different European regions, i.e. western Europe through westerly air masses and central Europe through (south-) easterly air masses (Lenschow et al., 2001). In winter, the latter are associated with cold, stagnant weather conditions (Spindler et al., 2004; Brüggemann et al., 2009; Engler et al., 2012). Recent receptor modelling results showed combustion and secondary inorganic aerosols, e.g. ammonium, nitrate and sulphate, to be the main source groups during such cold spells (van Pinxteren et al., 2019). The same conditions also cause large trans-boundary contributions

from Eastern European countries (van Pinxteren et al., 2019; Timmermans et al., 2020). As methodologies combining measurements and back trajectories as well as receptor models usually provide a limited number of source sectors and are less suitable to quantitively identify the source regions (Belis et al., 2020), one cannot rely on observations alone to quantify the relevant (geographic) source contributions.

Chemistry transport models (CTMs) are deterministic and can provide quantitative source attribution estimates, which is an advantage above qualitative results based on empirical studies (Potier et al., 2019). Numerous model studies have been carried out to point out the sources of PM and their composition (Hendriks et al., 2013; Garg & Sinha, 2017; Potier et al., 2019; Thunis et al., 2018). However, a prerequisite for using these modelling results is that they reproduce the observed concentration levels and their variability. Previous studies have highlighted the challenges of modelling PM episodes under stable conditions. Underestimation of the observed PM concentration can be related to insufficient treatment of temporal emission variability (Mues et al., 2014) or underestimation of residential wood combustion emissions (Spindler et al., 2004; van der Gon et al., 2015). In addition, the reliability of simulations with CTMs to quantify concentrations strongly depends on the quality of the meteorological input data (Vautard et al., 2012). A multi-model comparison for an winter episode in 2003 revealed a characteristic underestimation of the PM concentrations in modern CTMs (Stern et al., 2008). Parametrizations of the mixing layer height (MLH) in meteorological models are identified as one source of the underestimation of PM under stable conditions and shallow boundary layers as shown by Seibert et al. (2000). Still, only a few studies have addressed the improvement of planetary boundary layer (PBL) variables for use in air quality model simulations (Hu et al., 2010; Buzzi et al., 2011; Banks & Baldasano, 2016).

In this study we explore if we can improve the modelling of PM episodes during winter in east-Germany by high resolution nonhydrostatic meteorological modelling (dynamical downscaling) using the COSMO-CLM model. Sensitivity studies were conducted to investigate the representation of the PBL conditions. Meteorological quantities as the MLH were evaluated against radiosonde observations. The impact of different PBL parameterizations on modelled PM concentrations was analyzed. In addition, we investigated the impact of using two different vertical structures in the LOTOS-EUROS CTM. The impact of the dynamical downscaling was compared to the operational set-up of the LOTOS-EUROS CTM using the ECMWF meteorological driver.

2 Methodology

A dynamical downscaling approach with the COSMO-CLM model has been applied to generate high resolution meteorological input data for the LOTOS-EUROS CTM. First, we performed sensitivity studies to investigate the representation of the PBL conditions on the modelled PBL height and PM concentrations for January 2016. Accounting for the lessons learned, we applied the system to the next winter (September 2016 to March 2017) to further investigate and validate the impact of different horizontal and vertical set-ups. To assess the added value of the dynamical downscaling we used a simulation with meteorological input data of the ECMWF forecast model system (Flemming et al., 2009) as reference.

2.1 Study Area and Periods

The Berlin metropolitan area is the largest conurbation of Germany covering an area of 891 km². With more than 3.75 million inhabitants Berlin is densely populated. Berlin's dynamic population increase combined with a pronounced tourist impact of about 13.50 million visitors per year is reflected in the air pollution management plan by targeting e.g. the construction (agglomeration) and traffic sectors (SenStadt, 2019). Berlin is situated in the North German Plain

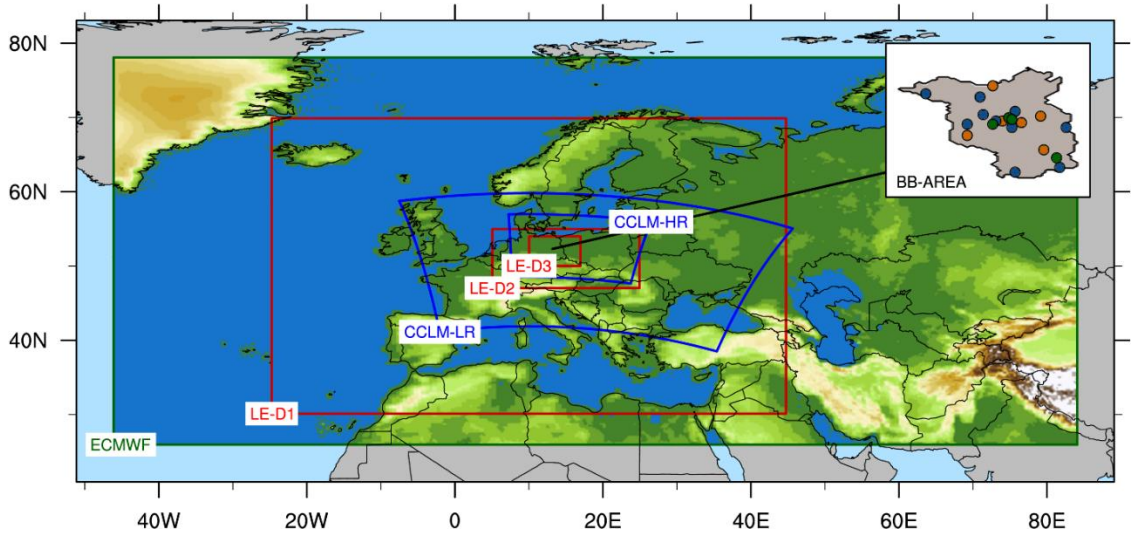

Fig. 1 Domain configuration of the model area. Three zooming domains are used for the LOTOS-EUROS CTM simulations (red). Meteorological boundary datasets are provided by the ECMWF model (green) and the COSMO-CLM (blue) model. As the COSMO-CLM model is applying a dynamical downscaling approach, two set-up areas are needed. The investigation area of Berlin Brandenburg (BB) is attached on the right-hand side and contains the location of the rural- (orange), suburban- (blue) and urban-background observation sites.

at 52°30' N and 13°30' E (Fig. 1). The neighboring republic of Poland is about 80 km from the eastern edge of the city. Berlin's conurbation is characterized by low orography features and intersected by the Spree valley. The average altitude above sea level is about 35-70 m increasing towards the border of the city. The maximum elevation is about 115 m. According to the prevailing season, Berlin is dominated by maritime climate in summer and continental climate in winter. The ambient air pollution in Berlin and its vicinity can be regarded as moderate. Annual average PM_{10} concentrations in 2016 ranged between 22.0 $\mu g/m^3$ and 26.8 $\mu g/m^3$ for urban background and traffic stations, respectively (SenStadt, 2019). Levels in the surrounding rural area are typically about 17.0 $\mu g/m^3$ and thus about 5.0 $\mu g/m^3$ lower than recorded in the urban background (LFU, 2018). In recent years, exceedances of daily mean limit values of the PM concentration were limited and have only been recorded at traffic locations (LFU, 2018; SenStadt, 2019).

This study focuses on two periods, i.e. January 2016 and September 2016 to March 2017. These periods were selected as they contain episodes exceeding the daily PM limit value, caused by cold and stable weather conditions (Fig. 2). January 2016 was selected as this month is split into two major periods differing in their meteorological conditions. The first cold spell in the first week (2^{nd} to 7^{th}) was characterized by an easterly wind inflow. Temperature minima down to -10.0° C were observed at the surface. A second (19^{th} to 22^{nd}) took place with a low-pressure system crossing inducing inversion layering. Temperatures during the westerly wind period reflect the typical variation of a frontal passage and therefore vary between 0°C and -10.5°C. Apart from the differing wind direction the meteorological conditions during both periods were quite similar. Low wind speeds were recorded for both periods resulting in a monthly mean of about 3.4 m/s at the surface. The MLH derived from radiosonde data was on average about 647 m and showed a large day-to-day variability. A PM episode with concentrations reaching values well above 90 ug/m^3 was observed from the 2^{nd} to the 7^{th}, (see Fig. 2). Despite similar meteorological conditions, during the westerly wind inflow period (19^{th} to 22^{nd}), no exceedances of the daily limit values were identified.

As the period of January 2016 is quite short, a second investigation period containing a winter PM episode has been examined. Therefore, the September 2016 to March 2017 was selected, with similar meteorological conditions compared to the reference period of January 2016 during wintertime of January to February 2017. The January to February 2017 was affected by low mixing and a mean mixing layer height of about 545 m. Mean temperatures were close to zero

with minima of about -10° C. The average wind speed below 3 m/s is quite low, whereas exceedances of the daily limit values again only occur during easterly wind periods. An advantage of investigating this winter is that we could use the data of the PM-OST campaign (van Pinxteren et al., 2019) for evaluating the modelled PM composition.

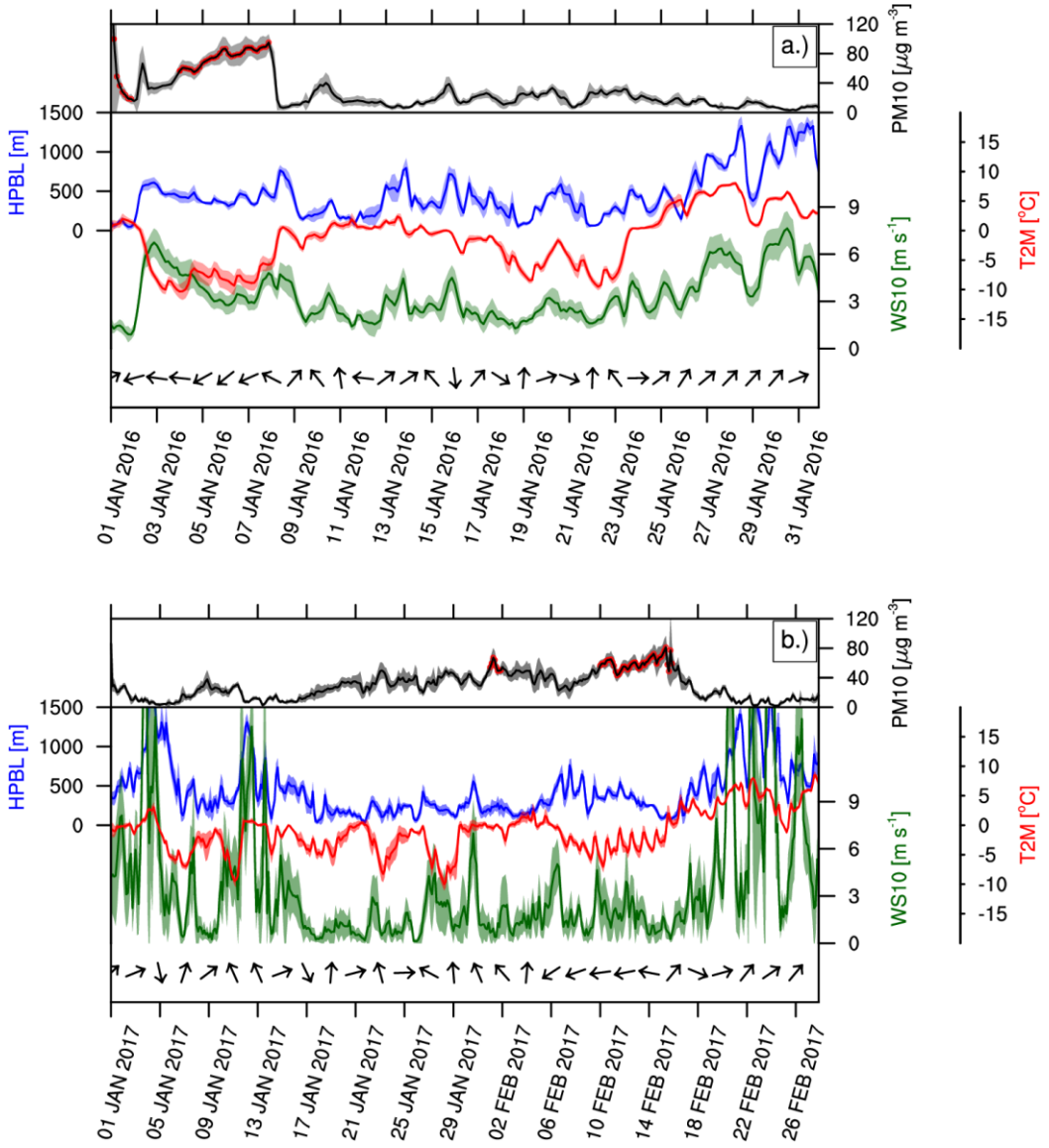

Fig. 2 Time series of investigation periods, representative for January 2016 (a) and January to February 2017 (b) for the Berlin agglomeration. PM mass concentration levels (black) are plotted on top with meteorological fields, as the mixing layer height (blue), the 2m-temperature (red), the 10m-wind-speed (green) and the 10m-wind-direction above. Red dots indicate exceedances of the daily limit value. Parameters representing the spatial average of all observation sites.

2.2 Nonhydrostatic Meteorological Modelling

A dynamical downscaling of the ERA-Interim reanalysis (Dee et al., 2011) was performed using the COSMO-CLM version 5.00 (Consortium for Small-Scale Modelling-Climate Limited-area Modelling) model (Doms et al., 2011; Doms & Baldauf, 2018) by using a double nesting approach. The first nested domain of the COSMO-CLM model (Fig. 1) covers Europe from 4° W down to 40° E and 42° N - 59° N with a horizontal resolution of 0.0625° (7 x 7 km²). The second nested domain covers Germany and Poland between 8° E - 25° E to 48° N - 57° N with a resolution of 0.025° (2.8 x 2.8 km²). Independent of the spatial resolution 40 vertical levels were used, with at least 11 levels below 1 km to be able to represent the vertical behavior in the PBL. The domain configuration was chosen to resemble the DWD COSMO-DE configuration to allow for future operational use of COSMO-DE to provide air quality forecasts.

The convective scale operational numerical weather prediction model COSMO-LM, was originally developed at the German Weather Service (DWD). The aim was to be able to simulate nonhydrostatic processes which appear on the meso-β and meso-γ scale. The model focuses on deep moist convection and severe weather events. In Rockel et al. (2008) a documentation of the COSMO-CLM, the climate mode of the COSMO-LM, is given. The climate mode is designed for longer simulation periods using numerous lateral boundary conditions (e.g. sea surface temperatures, vegetation parameters). COSMO-CLM is a limited-area model defined on spherical rotated geographical coordinates, following a generalized terrain height coordinate in the vertical. A staggered Arakawa C-grid is used to represent the orthogonal discretization (ARAKAWA & LAMB, 1977), with a Lorenz hybrid z-layering applied in the vertical (Herzog, Schubert, et al., 2002).

The representation of the PBL was investigated for January 2016 by an ensemble of turbulence parameterization schemes of the COSMO-CLM model (Tab. 1). Ranging from basic meso-β flow systems to more sophisticated ones, the spectra of turbulent closure approaches is broad. Three closure approaches of the vertical diffusion and two surface flux schemes are available in the COSMO-CLM model. A detailed description of the implemented parameterizations can be found in (Doms et al., 2011). In this study a combination of all 6 parameterizations have been applied (Tab. 1). The most simple closure approach as shown by Muller (1981) (1-D Diagnostic Closure) is based on the assumption of the boundary layer approximation neglecting horizontal turbulent

fluxes. Mellor & Yamada (1974) developed a more extensive second-order parameterization (1-D TKE-Based Diagnostic Closure), extended by Louis (1979) with a surface flux formulation for the Prandtl-layer dependent on stability and roughness-length. The most sophisticated closure approach (3-D TKE-Based Prognostic Closure) focuses on highly resolved LES-like model simulations of subgrid-scale processes to avoid current boundary layer approximations (Herzog, Schubert, et al., 2002; Herzog, Vogel, et al., 2002). According to Louis (1979) analytical functions are applied to solve the transfer coefficients of roughness length and stability parameters of the surface flux formulation based on the Businger relations (Businger et al., 1971) (Standard Bulk-Transfer Scheme). Based on the coefficients of the Mellor-Yamada closure, the second surface flux scheme applies two layers by using a transport resistance of the laminar turbulent roughness layer and a constant Prandtl-layer. As described in Doms et al. (2011) an advanced surface layer scheme (TKE-Based Surface Transfer Scheme) is implemented into COSMO-CLM relating to the Mellor-Yamada closure approach (Mellor & Yamada, 1974). The surface layer is sub-divided into roughness layer and Prandtl-layer. Additional control parameters like as the turbulent length and

Tab. 1

List of planetary boundary layer sensitivity parameterizations used in this work.

	Turbulence Scheme	**PBL Parameterization** **Surface Scheme**	**Tuning Parameter**
CCLM-TC-V1-1	1-D Diagnostic Closure	Standard Bulk-Transfer Scheme	-
CCLM-TC-V1-2		TKE-Based Surface Transfer Scheme	-
CCLM-TC-V2-1	1-D TKE-Based Diagnostic Closure	TKE-Based Surface Transfer Scheme	-
CCLM-TC-V2-2			lexpcor, ltmpcor, lcpfluc and ltkecon are applied
CCLM-TC-V2-3		Standard Bulk-Transfer Scheme	-
CCLM-TC-V3-1	3-D TKE-Based Prognostic Closure	TKE-Based Surface Transfer Scheme	-
CCLM-TC-V3-2			Reduction of the turbulent length scale (50 m)
CCLM-TC-V3-3			Lowering of the diffusion coefficient of heat (0.1 m^2s^{-1})
CCLM-TC-V3-4			Adopting both parameters used in V3-2 and V3-3

the diffusion coefficients of heat enlarge the range of possible configuration options. Different setups such as the impact of the turbulent heat and moisture fluxes and their reliance to condensation processes (lexpcor), the computation of thermal sources (ltmpcor) as well as the consideration of the convective buoyancy (ltkecon) for the TKE equation and variations in the heat capacity of air (lcpfluc) have been used as further test properties (Tab. 1). A more detailed description of the applied control parameters are available in the COSMO-CLM users guide (Schättler et al., 2019). For the winter of 2016-2017 we performed a single dynamical downscaling using the advised setup using the "1-D TKE-Based Diagnostic Closure" and the "TKE-Based Surface Transfer Scheme".

2.3 Chemical Transport Modelling

Air quality simulations were performed using the chemistry transport model (CTM) LOTOS-EUROS version 2.1 (Manders et al., 2017). LOTOS-EUROS is an open-source 3D CTM, developed at TNO (Netherlands Organisation for Applied Scientific Research) in cooperation with partners such as the FUB (Freie Universität Berlin). The aim of the model is to analyze and forecast air pollution concentrations in the lower troposphere. The model is part of the European regional ensemble of the Copernicus Atmospheric Monitoring Service (CAMS) (Marécal et al., 2015), providing operational forecasts and analyses for Europe. An important application of the model is for source apportionment in different regions worldwide, e.g. Netherlands, China, and Germany (Kranenburg et al., 2013; Timmermans et al., 2017, 2020).

LOTOS-EUROS is based on a regular Eulerian grid with variable horizontal resolution over Europe (Manders et al., 2017) and terrain following vertical coordinates. The gas-phase chemistry is solved with the TNO CBM-IV scheme, a simplified version of the original scheme by Whitten et al. (1980). The hydrolysis of N_2O_5 (Schaap et al., 2004) and the cloud chemistry sulfate formation (Banzhaf et al., 2012) are explicitly treated. Computations for aerosol chemistry are performed with the ISORROPIA-II module (Fountoukis & Nenes, 2007). Dry deposition processes for the gas-phase are derived based on the DEPAC (DEPosition of Acidifying Compounds) module (Wichink Kruit et al., 2012; Van Zanten et al., 2010). Dry deposition of particles is implemented using the scheme of Zhang et al. (2001). Wet deposition processes are solved as described by Banzhaf et al. (2012). The horizontal advection of pollutants is calculated

applying a monotonic advection scheme as shown by Walcek (2000). For a more detailed description of the LOTOS-EUROS model we refer to Manders et al. (2017) and references therein.

For Europe, a regional inventory of the CAMS emissions developed by the TNO for 2015 was applied. The GRETA (Gridding Emission Tool for ArcGIS, Schneider et al. (2016)) inventory is used for the German anthropogenic emission distribution (Tab. 2). A separate annual time profile for each source category represents the temporal variation that breaks down the annual emission totals. The CAMS fire product (Kaiser et al., 2012) provides information on wildfire emission sources. Chemical boundary conditions were taken from the Integrated Forecasting System provided by ECMWF (European Centre for Medium-Range Weather Forecasts) (C-IFS, Marécal et al. (2015)).

Tab. 2
Model runs and settings performed for the LOTOS-EUROS model.

		COSMO-CLM		**ECMWF IFS 12h forecasts**
Meteorological Input Data	**Spatial Resolution**	0.0625° x 0.0625° @ 7 x 7 km² (LR)	0.025° x 0.025° @ 2.8 x 2.8 km² (HR)	0.14° x 0.14° @ 15 x 15 km²
	Vertical Resolution	Lorenz hybrid z-level (40 layers)		3-layer-interval-averaged product of the ECMWF-L91 hybrid-sigma pressure levels (20 layers)
	Domain	4° W - 40° E to 42° N - 59° N	8° E - 25° E to 48° N - 57° N	46° W - 84° E to 26° N - 78° N
	PBL Sensitivity	See Tab. 2		/
Chemical Transport	**Spatial Resolution**	0.125° x 0.0625° @ 7 x 8 km² (D2)		0.0625° x 0.03125° @ 4 x 4 km² (D3)
	Vertical Structure	Multi layering approach @ 15 layers up to 2 km	Mixed layer approach @ 5 layers up to 5 km	Multi layering approach @ 15 layers up to 12 km

Domain	5° E - 25° E to 47° N - 55° N	10° E - 12° E to 50° N - 54° N
Period	January 2016	September 2016 – March 2017
Boundary Conditions	LOTOS-EUROS climatological simulation with ECMWF IFS 12 h forecast conditions (0.5° x 0.25° @ 28 x 32 km²)	
Anthrop. Emissions	CAMS-RWC-AP 2015 (v1.1) and CAMS-2015-RWC-update-GrETa-gridding (v.1.1)	

The standard meteorological input data of the LOTOS-EUROS CTM is derived from the operational meteorological dataset of the IFS (Integrated Forecasting System) provided by the ECMWF (Flemming et al., 2009). The meteorological forecasts offer a spatial resolution of about 0.14°, with hybrid-sigma pressure layers define the vertical coordinate system (Eckermann, 2009). The vertical resolution of the input data corresponds to a selection of 20 layers by vertical interval averaging of 3 layers derived from the ECMWF-L91 product, with the lowest level matching the initial layer of the ECMWF meteorology. The meteorological forecast is stored to enable re-analyses of past periods. The ECMWF data cover Europe from 46° W down to 84° E and 26° N - 78° N (Fig. 1).

The standard approach for increasing resolution by nesting the LOTOS-EUROS air pollution modelling is performed by a statistical downscaling of the ECMWF meteorological input data. In this study an interface between COSMO-CLM and LOTOS-EUROS was developed to make further use of the dynamically downscaled COSMO-CLM meteorology. To implement the meteorological input data of the COSMO-CLM model, the spherical rotated horizontal and the hybrid z-layering vertical grid information's has been described within the LOTOS-EUROS CTM. A corresponding specification of the transformation of the available COSMO-CLM variables into the required fields within the LOTOS-EUROS CTM was performed like it was already implemented for the ECMWF model (Manders et al., 2017) and for the WRF model (Escudero et al., 2019). Both the horizontal and vertical grid configuration correspond to the model specification as provided by the DWD model family, avoiding interpolation of the data. The LOTOS-EUROS simulations were performed for three different regions and spatial resolutions using a one-way nesting approach (Fig. 1). The large scale European simulation (28 x 32 km²) was performed with

ECMWF meteorology, the higher resolution nests over Germany-Poland (7 x 8 km²) and East-Germany (4 x 4 km²) were performed by both meteorological drivers (Fig. 1).

Two concepts of the vertical structure were tested in the LOTOS-EUROS CTM. The current operational LOTOS-EUROS model set-up uses a dynamic mixed layer approach (MIX) consisting of 5 layers extending up to 5 km above sea level to determine the vertical (Manders et al., 2017). The vertical is structured by using a static surface layer of 25 m followed by a dynamic layer. The height of the dynamic layer equals the MLH, derived by the meteorological input data. Up to 3.5 km two equally thick dynamic reservoir layers are implemented. Hence, the depth of the vertical layers varies in time and space. To resolve free tropospheric transport processes like mineral dust transport, a fifth layer exceeding the 3.5 km altitude is used. As prerequisite for applying the dynamic mixed layer approach a homogenous pollutant distribution is presumed within the PBL. However, assuming a well-mixed PBL can lead to a wrong representation of the vertical mixing in the model system. Due to deep reservoir layers overestimated mixing, particular during stable weather conditions with low MLHs, occurs. Therefore, recent model developments apply a much larger number of vertical layers in the LOTOS-EUROS CTM to reproduce the vertical structure of the planetary boundary layer (Escudero et al., 2019) and to provide a better understanding of the vertical distribution of pollutants, the multi-level version (MUL) negates the assumption of a well-mixed PBL and better accounts for the residual layer dynamics. The multi-level model version uses the vertical level information as provided by the meteorological input data. Here, the multi-level approach of LOTOS-EUROS was applied using the lowest 15 hybrid z-level of COSMO-CLM and hybrid-sigma pressure layers of the ECMWF as input data.

2.4 Observational Data and Metrics

The meteorological simulations were evaluated compared to radiosonde observation from Lindenberg, Schleswig, Greifswald in Germany and Leba, Legionowa and Wroclaw in Poland. To compare to both meteorological model systems, the radiosonde observations were vertically interpolated to the corresponding model layering. To derive the MLH for both, observations and model results, the bulk Richardson method was used (Seibert et al., 2000). Defined as an dimensionless quantity and used in the turbulent kinetic energy (TKE) equation, the bulk Richardson number describes the bulk-ratio of the buoyant consumption term and the mechanical production term (Stull, 1988). The MLH refers to the altitude at which the bulk Richardson number

is reaching a pre-set threshold, known as the critical Richardson number. Critical values of 0.2 to 1.0 are indicated in literature. Here we used the COSMO-CLM thresholds of 0.33 at stable conditions (Wetzel, 1982) and 0.22 during convection (Vogelezang & Holtslag, 1996) to determine the MLH based on the thermo-dynamical parameters and moisture variables.

To evaluate the modelled PM mass concentrations, observation data were collected from the ground-based monitoring networks in Germany collected by the German Environment agency UBA (www.uba.de). As we evaluated relatively short time periods, we chose to ensure full data coverage by using monitoring sites with 99% data availability. Traffic sites were neglected as these are not representative for the model resolution. The monitoring sites were clustered into rural-background (6), suburban-background (10) and urban-background (4). To determine the contribution of individual components to the total PM concentration, data from the PM-OST monitoring campaign were used (van Pinxteren et al., 2019). The spatial-temporal mass concentration characteristics were illustrated by box plots. Mean diurnal and weekly cycles were calculated for all sites clustered by station type to examine the temporal variability of modelled and measured mass concentration. When analyzing the mass concentration per station type the data for all stations within a type were averaged in advance. To quantify the impact of meteorological conditions on the PM mass concentration level, a classification was carried out. The classification is based on three meteorological quantities. 2m-temperature ($T_C \leq 273.15$ K and $T_W > 273.15$ K), 10m-wind speed ($WS10_L \leq 3.3$ m/s and $WS10_H > 3.3$ m/s) and 10m-wind direction (WD10 [0°…360°, 90°]). Equally sized clusters were defined by using a bootstrapping algorithm. To include vertical mixing, the classified PM concentration data were plotted against the MLHs of both meteorological input data sets. To assess the different model configurations used in this study, model statistics based on Chang & Hanna (2004) were used.

3 Results

3.1 January 2016

A comparison of both meteorological data from COSMO-CLM and ECMWF against radiosonde data was carried out for January 2016 before investigating the impact on the chemical transport modelling. Here we focus on thermodynamic parameters such as the MLH, temperature

and wind speed. To evaluate the COSMO-CLM model, an ensemble of the PBL parameterization simulations is used.

Observed temperature profiles of the lower PBL are rather well captured by both meteorological input datasets (Fig. 3, left). The ensemble of the COSMO-CLM model predicts systematically lower temperatures in the model domain compared to the ECMWF model, with an underestimation of observed values increasing towards the surface. The ECMWF model overestimates the temperatures compared to observations, most pronounced above the 700 m altitude. The structure of the vertical profile in the observations is considerably better reflected by the COSMO-CLM ensemble than the ECMWF model. Both models do not represent the cold easterly wind inflow period as well as the westerly wind inflow period.

For wind speed both meteorological datasets show a striking underestimation (of up to a factor of three) of the measured values (Fig. 3, right). The underestimations are visible over the entire vertical of the PBL and are most pronounced at about the 700 m altitude. The ensemble of the COSMO-CLM model provides higher wind speeds and a closer resemblance of the observed profile than the ECMWF model.

In general, the MLHs (Fig. 4) derived from both model simulations are lower compared to those derived from radiosonde measurements. The monthly mean bias of the ECMWF model is about -226 m and about -123 m for the COSMO-CLM ensemble mean. This could be attributed to an insufficient representation of the sensible and latent heat flux of the used model systems in the target area, which leads to lower near surface temperature estimates compared to the observations and the subsequent formation of inversion layers. Further research studies are required to investigate this issue. Deviations from the mean provide information of the variability and the temporal evolution. With this respect a large spatial variability between observation sites can be recognized, with the largest variation appearing in Leba. A rather good representation of the temporal evolution, with a correlation coefficient of 0.76, can be achieved using the COSMO-

CLM ensemble. The ECMWF model, on the other hand, has weaknesses representing the temporal

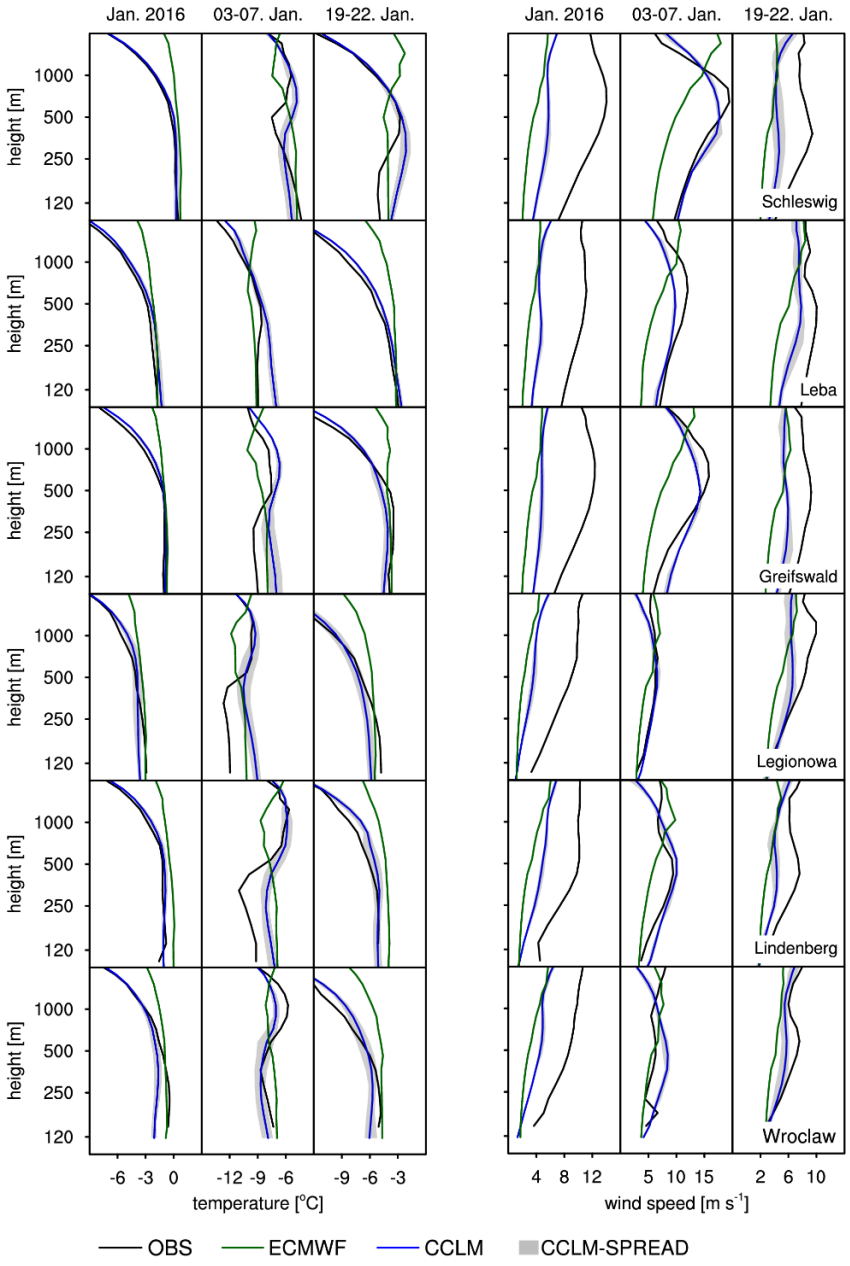

Fig. 3 Profiles of the temperature (left hand side) and the wind-speed (right hand side) for January 2016, split into sub-periods of 01.-31., 03.-07. and 19.-22. 01. 2016. Observation data are selected out of radiosonde measurements at Schleswig, Leba, Greifswald, Legionowa, Lindenberg and Wroclaw and color-coded in black. Model simulations are color-coded in green (ECMWF) and blue (COSMO-CLM). The COSMO-CLM model data is plotted as ensemble mean of the boundary layer parameterizations with their related spread marked as grey area.

evolution (correlation coefficient 0.13) of the MLH. The main weakness of both models is indicated by the standard deviation of the MLH. Even though the standard deviation of the

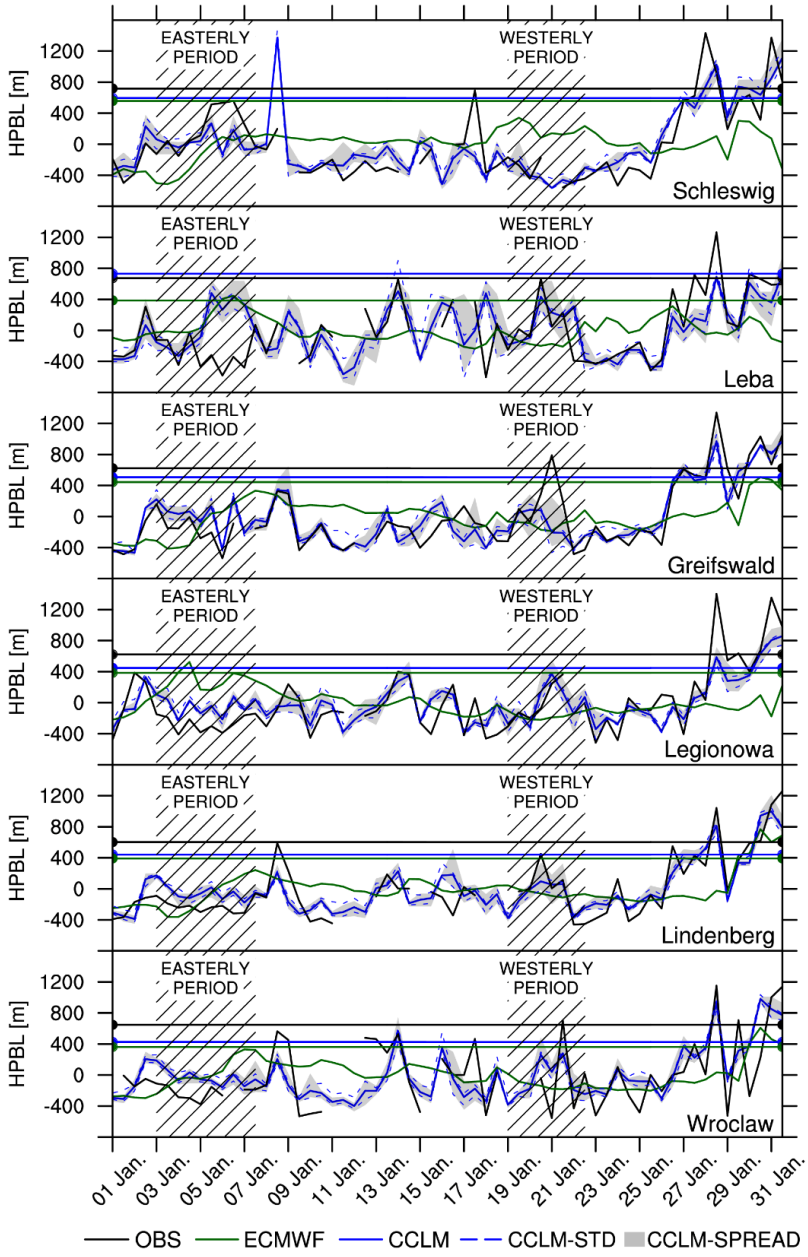

Fig. 4 Time series of the mixing layer height and deviation from mean, for January 2016. Observations are derived from radiosonde data in Schleswig, Leba, Greifswald, Legionowa, Lindenberg and Wroclaw is color-coded in black. Meteorological boundary data is color-coded in green (ECMWF) and blue (COSMO-CLM). The COSMO-CLM data is plotted as ensemble mean of the boundary layer parameterizations, the related spread marked as grey area and with the standard deviation coded as dashed line.

COSMO-CLM ensemble MLH is closer to the observation, modelled values (about 340 m) are lower than observed (424 m). A noticeable lower standard deviation around the mean MLH is computed for the ECMWF model (189 m). Hence, the dynamical downscaling using COSMO-CLM provides improved meteorological information compared to the standard dataset from ECMWF.

The impact of different PBL parameterizations of the COSMO-CLM model can be regarded as small (grey area in Fig. 3). Main impact can be noted in the lower atmosphere, with largest differences near the surface compared to the ensemble mean, which can be explained by a lower vertical layer thickness near the surface. Lowering the diffusion coefficient of heat leads to cooler conditions with increased wind speeds, whereas e.g. the 3-D TKE-based prognostic closure approach leads to a warming in the PBL. Largest differences with a temperature variance of about 1 K can be observed especially during cooling events. Changes in wind speed are about 1 m/s during the PM episode and about 0.5 m/s for the entire month. The MLH and the corresponding temporal evolution are not significantly affected (see grey area in Fig. 4). Although the spread between members is up to 200 m and thus comparatively large, no single ensemble member provides a consistent indication of a better performance in representing the PBL meteorology.

Below, the COSMO-CLM ensemble and the reference ECMWF data are used to drive the LOTOS-EUROS CTM.

Monthly mean PM mass concentration levels in the rural background during January 2016 were about 24 $\mu g/m^3$ (see Fig. 5 and Tab. 3). The LOTOS-EUROS CTM simulations fed with the COSMO-CLM ensemble underestimate the observed concentrations by 8.1 $\mu g/m^3$ on average. The modelled variability is much lower than observed in reality. This can be explained by an overestimation during the westerly wind period of about 0.5 $\mu g/m^3$, and a relatively large underestimation during the easterly wind regime (up to -43.6 $\mu g/m^3$). Despite of a similar meteorological situation with a stagnant weather condition, this discrepancy can be explained by a high transboundary PM contribution. The simulations with the COSMO-CLM ensemble of PBL parameterizations do not provide large differences in the modelled PM mass concentration (Tab. 3). On average, PM levels modelled by individual members are deviating less than 0.4 $\mu g/m^3$ from the ensemble mean (Fig. 5). The model performance statistics for the ensemble mean of all LOTOS-EUROS simulations show small positive impacts on the temporal correlation and the

normalized mean squared error compared to the individual simulation members (Tab. 3). In Table 3 we also compare the validation statistics of simulations using ECMWF and different model resolutions. Using ECMWF meteorological data instead of COSMO-CLM provides larger correlation coefficients and lower error statistics. Independent on meteorological driver the vertical structure leads to a substantial increase in levels and modelled variation. The increase in horizontal resolution (D3 vs D2) leads to a slightly larger increment between rural and urban sites.

In short, the impacts of the COSMO-CLM ensemble (members) is small compared to the use of different meteorological input data (COSMO-CLM vs ECMWF) and using different vertical model resolutions. The latter are discussed in more detail below for the winter 2016-2017, for which we did not pursue to perform the full ensemble calculations.

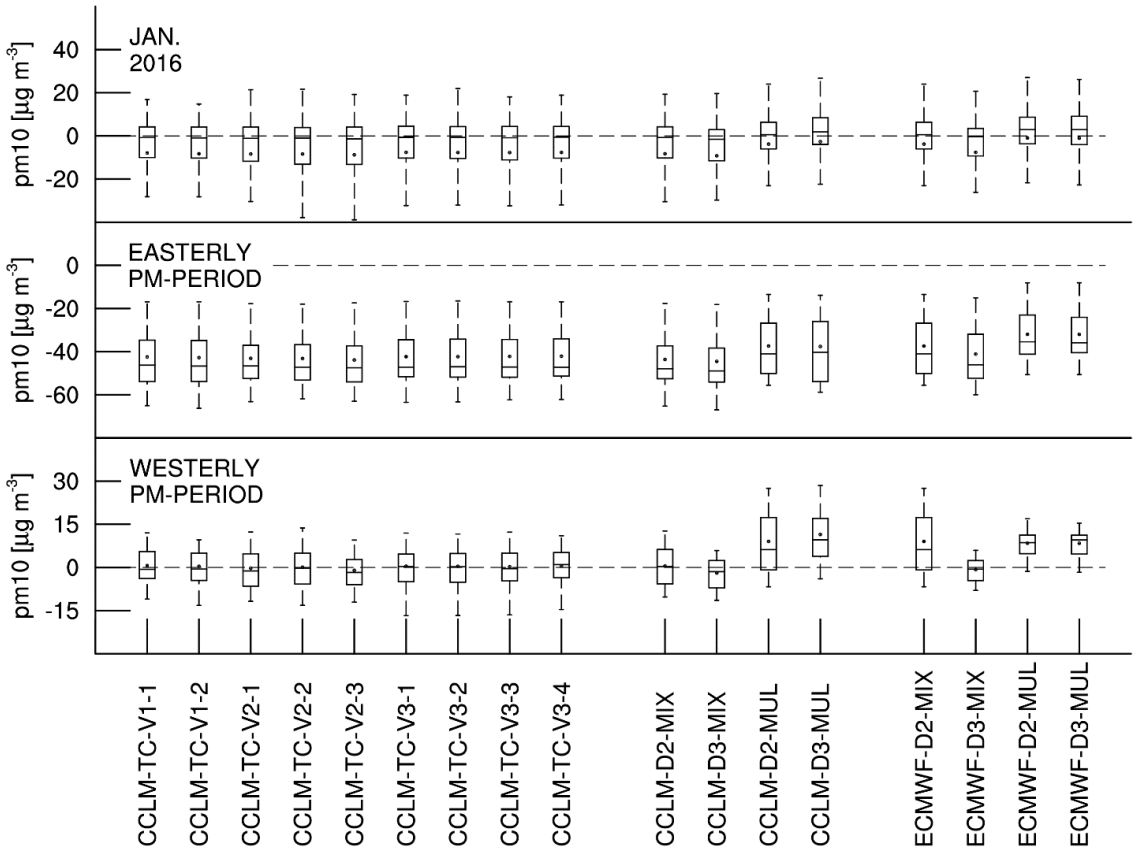

Fig. 5 PM mass concentration of the LOTOS-EUROS CTM dependent on the meteorological boundary conditions, the boundary layer parameterization, the horizontal resolution, and the vertical grid structure for the Berlin agglomeration. Three sub-periods have been investigated and are presented from top to bottom (01.-31., 03.-07. and 19.-22. 01. 2016).

Tab. 3

Statistics on modelled and observed means (μ), standard deviation (σ), temporal correlation coefficient (R_T), spatial correlation coefficient (R_S), geometric mean bias (MG), normalized mean square error (NMSE), geometric variance (VG), fractional bias (FB) and number of sites (NoS) for January 2016.

			$\mu_{mod} \pm \sigma_{mod}$	$\mu_{obs} \pm \sigma_{obs}$	R_T	R_S	VG	MG	NMSE	FB	NoS
COSMO-CLM	MIX	D2	15.70 ± 06.43	23.99 ± 21.76	0.53	0.52	1.68	1.25	1.16	0.42	6 RUBG
			15.23 ± 06.20	27.26 ± 25.61	0.50	0.53	1.74	1.46	1.64	0.57	10 SUBG
			20.08 ± 09.47	31.88 ± 35.17	0.24	0.88	1.80	1.36	2.03	0.45	4 URBG
		D3	14.77 ± 06.19	23.99 ± 21.76	0.55	0.59	1.72	1.34	1.27	0.48	6 RUBG
			14.16 ± 05.50	27.26 ± 25.61	0.51	0.58	1.82	1.57	1.82	0.64	10 SUBG
			21.31 ± 10.74	31.88 ± 35.17	0.17	0.94	1.82	1.28	1.96	0.40	4 URBG
		ENS	15.93 ± 06.63	23.99 ± 21.76	0.58	0.53	1.62	1.24	1.09	0.40	6 RUBG
			15.55 ± 06.36	27.26 ± 25.61	0.51	0.57	1.69	1.44	1.57	0.55	10 SUBG
			20.18 ± 09.49	31.88 ± 35.17	0.26	0.89	1.76	1.35	2.00	0.45	4 URBG
	MUL	D2	20.20 ± 11.41	23.99 ± 21.76	0.56	0.65	1.42	1.06	0.70	0.17	6 RUBG
			19.75 ± 11.29	27.26 ± 25.61	0.50	0.64	1.42	1.24	1.02	0.32	10 SUBG
			23.32 ± 13.14	31.88 ± 35.17	0.36	0.90	1.42	1.24	1.55	0.31	4 URBG
		D3	21.33 ± 11.31	23.99 ± 21.76	0.51	0.71	1.43	0.98	0.70	0.12	6 RUBG
			20.92 ± 10.99	27.26 ± 25.61	0.47	0.74	1.38	1.15	0.95	0.27	10 SUBG
			26.09 ± 14.07	31.88 ± 35.17	0.28	0.94	1.48	1.08	1.43	0.20	4 URBG
ECMWF IFS	MIX	D2	20.15 ± 06.69	23.99 ± 21.76	0.62	0.64	1.42	1.17	1.00	0.37	6 RUBG
			16.72 ± 06.66	27.26 ± 25.61	0.57	0.62	1.46	1.31	1.35	0.48	10 SUBG
			19.39 ± 08.51	31.88 ± 35.17	0.36	0.88	1.56	1.35	2.01	0.49	4 URBG
		D3	16.35 ± 06.76	23.99 ± 21.76	0.64	0.72	1.41	1.17	0.99	0.38	6 RUBG
			16.77 ± 06.67	27.26 ± 25.61	0.60	0.58	1.45	1.31	1.30	0.48	10 SUBG
			20.12 ± 08.98	31.88 ± 35.17	0.36	0.95	1.54	1.31	1.91	0.45	4 URBG
	MUL	D2	23.02 ± 11.00	23.99 ± 21.76	0.67	0.86	1.35	0.87	0.50	0.04	6 RUBG
			22.91 ± 11.05	27.26 ± 25.61	0.60	0.69	1.30	1.00	0.73	0.17	10 SUBG
			24.61 ± 12.00	31.88 ± 35.17	0.46	0.95	1.33	1.10	1.32	0.26	4 URBG
		D3	22.95 ± 11.00	23.99 ± 21.76	0.67	0.93	1.35	0.87	0.50	0.05	6 RUBG
			23.00 ± 11.08	27.26 ± 25.61	0.61	0.61	1.29	1.00	0.70	0.18	10 SUBG
			24.98 ± 12.14	31.88 ± 35.17	0.46	0.95	1.33	1.08	1.30	0.24	4 URBG

3.2 September 2016 to March 2017

3.2.1 Meteorological Input Data

Classifying the PM concentration by meteorological conditions for September 2016 to March 2017, more detailed information can be obtained on their relationship to thermodynamical quantities. Figure 6 illustrates the well-known feature of high PM concentration levels

predominant during cold periods when a shallow mixing layer is observed. By contrast, a low mass concent ration is evident during relative mild winter periods. Periods with weak wind speeds are linked to local impacts like urban emissions, high wind speeds are associated to long-range transport. Concentration levels are higher at south-east wind directions than at north-west ones in the investigation area of Berlin. Summarizing, high concentration levels in Berlin can be linked to long-range transport of air masses from East-European countries, during cold stagnant conditions. PM concentrations during westerly wind periods are well represented while an underestimation of PM concentrations is present for all mixed-layer model versions during easterly wind periods with respect to the UBA measurements. Warm periods are better reproduced than colder episodes. Largest PM underestimations for September 2016 to March 2017 are obvious for conditions with

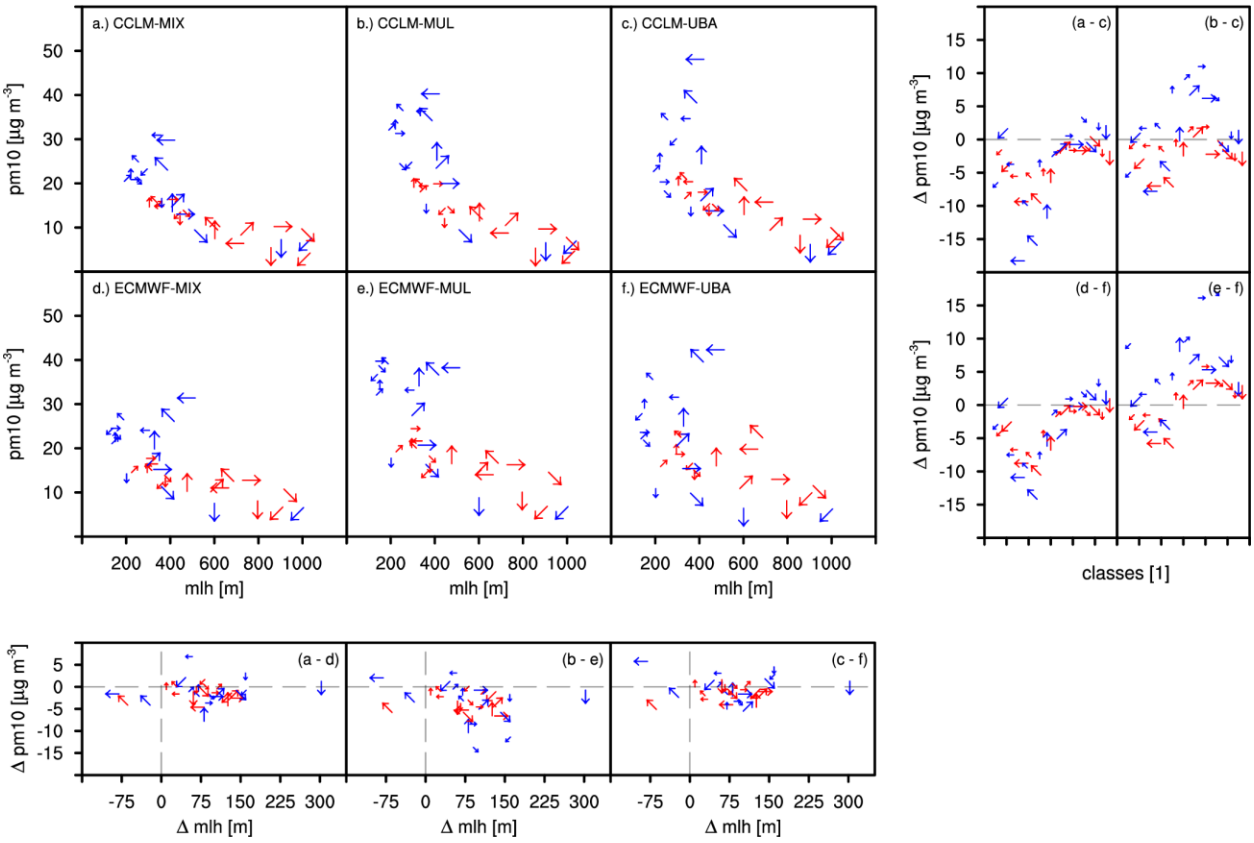

Fig. 6 Modelled (left: mixed layer approach [MIX], middle: multi-layering concept [MUL]) and observed (right) PM mass concentration levels are plotted over the MLH (a-f) for September 2016 to March 2017. Rural-background sites are used as evaluation sites, with the COSMO-CLM model (top) and ECMWF model (bottom) representing the meteorological boundary data. The PM mass concentration levels are divided into different classes depending on the meteorological condition. Anomalies of the different configurations are plotted on each side. The temperature impact is color-coded: $T_C \leq 273.15K$ as blue and $T_W > 273.15K$ as red. Wind speed is marked by the arrow length: $WS10_L \leq 3.3m/s$ and $WS10_H > 3.3m/s$. The wind direction is associated to the arrow direction: WD10 [0°...360°, 90°].

cold south-easterly high wind periods by up to 15.0 µg/m^3 compared to the observation. LOTOS-EUROS CTM simulations driven by the COSMO-CLM model and ECMWF input data differ, depending on the meteorological condition, in their mean MLH by about 75 m with the ECMWF model providing lower values for most of the time. Related PM mass concentration levels vary within 5.0 µg/m^3, with largest deviations during cold periods. Simulation results of the LOTOS-EUROS CTM using input data of the COSMO-CLM model are on average about -1.4 µg/m^3 lower in rural areas than ones computed by using the ECMWF model, with the more striking difference of about -7.4 µg/m^3 evident during cold stagnant PM episodes, which could be related to higher wind speeds of the COSMO-CLM model.

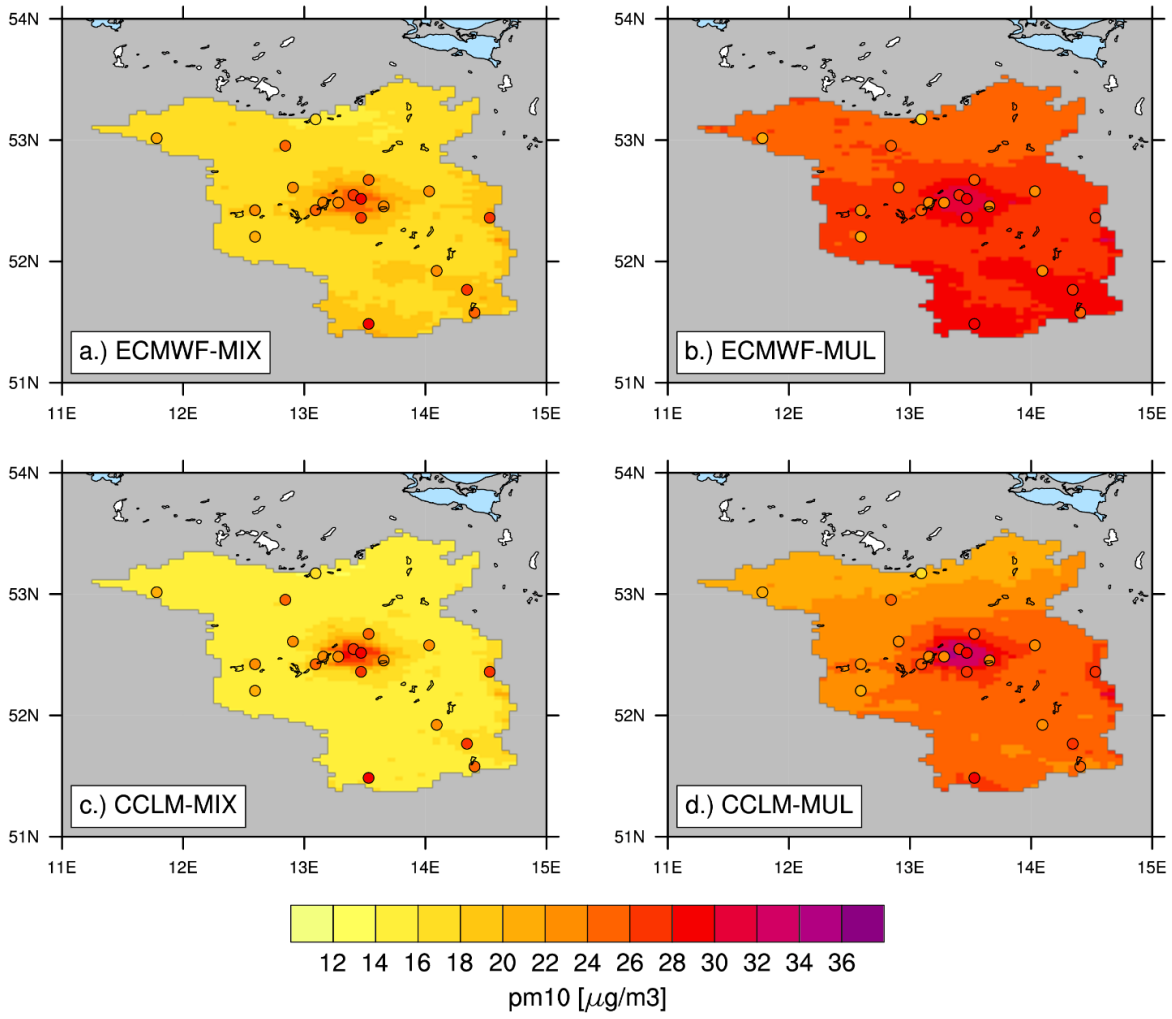

Fig. 7 Map of the observed (dots) and the modelled (ECMWF-MIX: a, ECMWF-MUL: b, COSMO-CLM-MIX: c and COSMO-CLM-MUL: d) PM mass concentration level for December 2016 to February 2017.

For winter December 2016 to February 2017, the monthly mean rural background concentration was 21.7 $\mu g/m^3$, with the major impact attributed to urban agglomerations of about 27.4 $\mu g/m^3$ (Fig. 7 and Tab. 4). This corresponds to an urban increment of about 5.7 $\mu g/m^3$. The rural background concentration levels for the mixed-layer model versions are underestimated by about -2.7 $\mu g/m^3$ on average with respect to the UBA measurements. Especially urban background (-5.2 $\mu g/m^3$) influenced areas cannot be captured by the LOTOS-EUROS CTM. Therefore, the modelled urban increment is underestimated by about 3.2 $\mu g/m^3$ on average. The average urban increment of the COSMO-CLM model system, applying the dynamical downscaling approach, lowers the underestimation of the increment of modelled PM mass concentration levels in the LOTOS-EUROS CTM seen in UBA measurements (Fig. 7). This particularly affects the enhanced

Tab. 4

Statistics on modelled and observed means (μ), standard deviation (σ), temporal correlation coefficient (R_T), spatial correlation coefficient (R_S), geometric mean bias (MG), normalized mean square error (NMSE), geometric variance (VG), fractional bias (FB) and number of sites (NoS) for December 2016 to February 2017.

			$\mu_{mod} \pm \sigma_{mod}$	$\mu_{obs} \pm \sigma_{obs}$	R_T	R_S	VG	MG	NMSE	FB	NoS
COSMO-CLM	MIX	D2	18.55 ± 09.75	21.67 ± 14.89	0.72	0.54	1.37	1.09	0.29	0.16	6 RUBG
			18.39 ± 09.52	24.71 ± 16.27	0.76	0.29	1.36	1.25	0.35	0.29	10 SUBG
			23.01 ± 12.62	27.36 ± 18.69	0.65	0.76	1.36	1.15	0.35	0.17	4 URBG
		D3	17.50 ± 08.84	21.67 ± 14.89	0.71	0.59	1.38	1.13	0.35	0.21	6 RUBG
			17.24 ± 08.41	24.71 ± 16.27	0.75	0.24	1.39	1.30	0.45	0.36	10 SUBG
			23.86 ± 12.74	27.36 ± 18.69	0.57	0.78	1.38	1.08	0.39	0.14	4 URBG
	MUL	D2	24.45 ± 15.64	21.67 ± 14.89	0.77	0.74	1.36	0.93	0.22	-0.12	6 RUBG
			24.38 ± 15.54	24.71 ± 16.27	0.80	0.43	1.28	1.06	0.17	0.01	10 SUBG
			28.32 ± 18.42	27.36 ± 18.69	0.71	0.78	1.32	1.03	0.26	-0.03	4 URBG
		D3	25.92 ± 15.43	21.67 ± 14.89	0.76	0.80	1.34	0.85	0.23	-0.18	6 RUBG
			25.68 ± 15.04	24.71 ± 16.27	0.79	0.50	1.24	0.97	0.17	-0.03	10 SUBG
			30.88 ± 18.32	27.36 ± 18.69	0.67	0.79	1.29	0.90	0.28	-0.12	4 URBG
ECMWF IFS	MIX	D2	18.93 ± 09.49	21.67 ± 14.89	0.76	0.63	1.25	1.06	0.25	0.14	6 RUBG
			19.55 ± 09.68	24.71 ± 16.27	0.80	0.41	1.23	1.16	0.28	0.23	10 SUBG
			22.20 ± 11.68	27.36 ± 18.69	0.69	0.66	1.26	1.17	0.34	0.21	4 URBG
		D3	18.86 ± 09.45	21.67 ± 14.89	0.76	0.68	1.25	1.06	0.26	0.14	6 RUBG
			19.41 ± 09.52	24.71 ± 16.27	0.80	0.41	1.22	1.16	0.29	0.25	10 SUBG
			23.02 ± 12.33	27.36 ± 18.69	0.67	0.78	1.26	1.13	0.34	0.17	4 URBG
	MUL	D2	28.04 ± 16.54	21.67 ± 14.89	0.76	0.84	1.30	0.74	0.27	-0.26	6 RUBG
			28.28 ± 15.86	24.71 ± 16.27	0.81	0.59	1.20	0.82	0.16	-0.13	10 SUBG
			30.06 ± 18.45	27.36 ± 18.69	0.67	0.79	1.20	0.88	0.29	-0.09	4 URBG

D3	27.70 ± 16.18	21.67 ± 14.89	0.76	0.87	1.30	0.74	0.26	-0.24	6 RUBG
	27.98 ± 15.69	24.71 ± 16.27	0.81	0.61	1.19	0.83	0.16	-0.12	10 SUBG
	30.44 ± 19.02	27.36 ± 18.69	0.64	0.85	1.21	0.87	0.32	-0.11	4 URBG

PM mass concentration levels of urban agglomerations. More gradients are visible in the PM distribution across highly polluted areas such as Berlin. Whereas the rural background concentration estimates for winter December 2016 to February 2017 are slightly higher by using the COSMO-CLM model compared to the observations (bias of -3.1 µg/m^3) than those of the ECMWF model system. In the urban background area, an underestimation of -4.4 µg/m^3 is obvious with respect to the observations. This results in an urban increment of 4.4 µg/m^3.

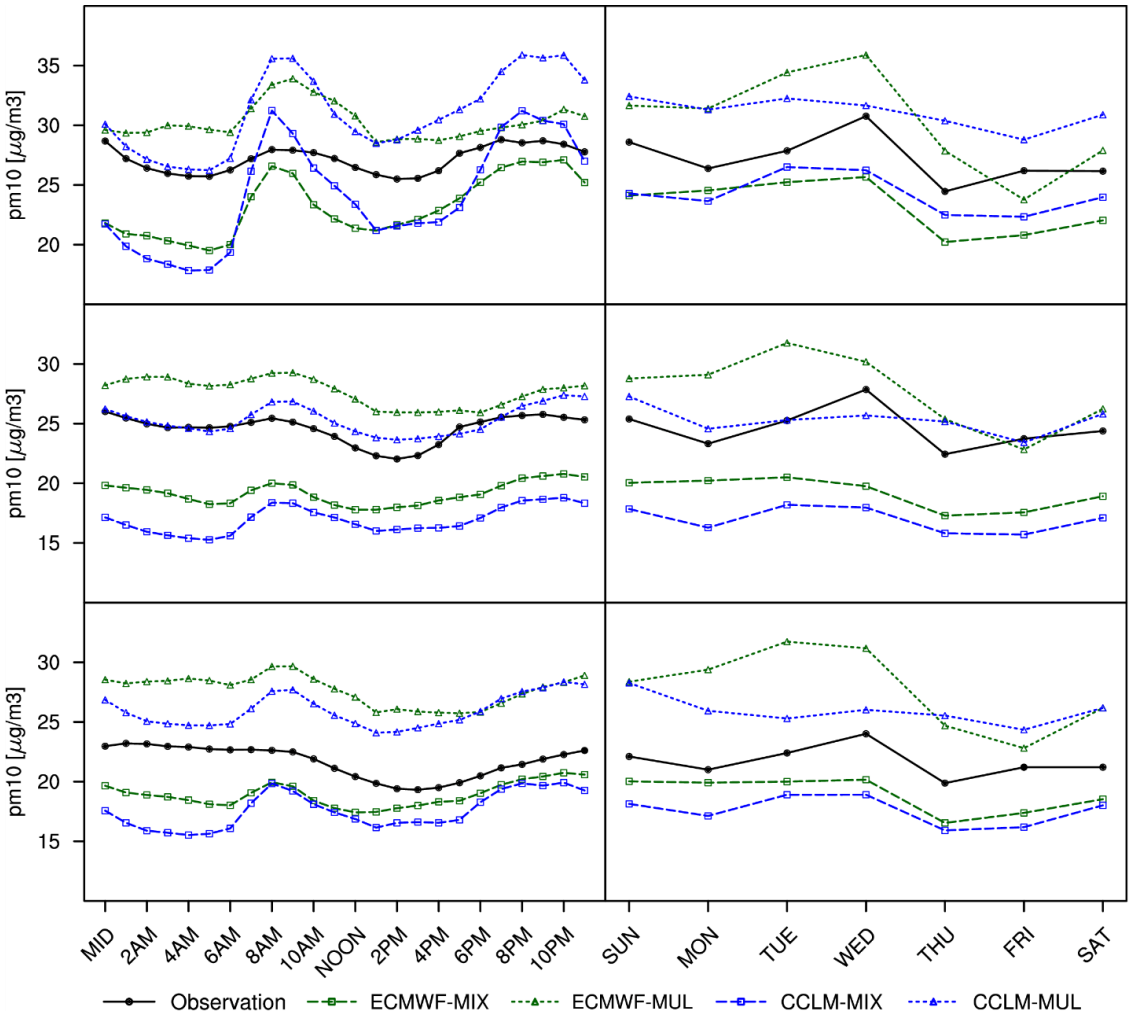

Fig. 8 Diurnal (left) and weekly (right) cycle of the observed (black solid line) and the modelled (green: dashed line – ECMWF-MIX, dotted line – ECMWF-MUL; blue: dashed line – COSMO-CLM-MIX, dotted line – COSMO-CLM-MUL) PM mass concentration levels for December 2016 to February 2017, split into urban- (top), suburban- (mid) and rural-background (bottom) areas.

Figure 8 provides observed and modelled diurnal and weekly cycles of surface PM concentration levels for winter December 2016 to February 2017. The observed diurnal cycle is characterized by a minimum during lunchtime and a maximum at night, caused by the natural development of the MLH. Whereas, in the urban area two peak values are observed during daytime, between 8-11 GMT and 19-22 GMT, mainly attributed to the impact of traffic rush hours and heating in conurbation areas. Diurnal cycles are too pronounced in the LOTOS-EUROS CTM simulations. Lower concentration levels are predominant in the early morning hours from midnight to 6:00 GMT, with about -5.5 $\mu g/m^3$ in rural areas and about -6.8 $\mu g/m^3$ in the urban background compared to the observation. Towards the evening the bias is reduced to about -3.5 $\mu g/m^3$ in rural areas and about -2 $\mu g/m^3$ in the urban background with respect to the UBA measurements. The mean correlation of the diurnal cycle for urban sites is 0.81, with simulations driven by COSMO-CLM input data showing smaller correlation coefficients by about 0.07. The more pronounced overshooting of peak concentration levels in urban areas by using the COSMO-CLM model reduces the temporal correlation to 0.57. Overall higher correlations can be provided using the ECMWF input data in the rural and sub-urban background area by about 0.05.

As the impact for different horizontal (D2 vs. D3) and vertical resolutions (MIX vs. MUL) of the LOTOS-EUROS CTM simulations is similar for varying meteorological input-data, we will focus on the COSMO-CLM model system.

3.2.2 Model Resolution

Differences by increasing the horizontal resolution are particularly evident when applying the dynamical downscaling approach of the COSMO-CLM model, with the major benefit of the higher resolution recognized in a more detailed representation of the spatial concentration distribution. For instance, increasing the horizontal resolution applying the zooming approach of the LOTOS-EUROS CTM (D2 to D3) is slightly affecting the PM mass concentration and reduces the rural background levels of the LOTOS-EUROS CTM model (Tab. 4 and Fig. 7). On average lower values of -1.1 $\mu g/m^3$ were computed compared to the coarser resolution for winter December 2016 to February 2017. In contrary, the concentration amount in the urban background of the LOTOS-EUROS CTM is increased by about 0.9 $\mu g/m^3$ when increasing the resolution from 7 km to 2 km. This increases the urban increment to about 6.4 $\mu g/m^3$. Simulation results show that

different horizontal resolutions applying different vertical structures delivered similar results, thus for the remainder discussions we will stick with the higher resolved model version.

Changing the vertical structure (MIX vs. MUL) of the LOTOS-EUROS CTM exhibits a larger impact than increasing the horizontal resolution. By applying the multi-level approach, higher levels of the PM mass concentration are obvious in almost all meteorological conditions with respect to the mixed layer approach (Fig. 6). The multi-level version leads to a considerably reduction of the underestimation during cold south-easterly high wind periods from -14 $\mu g/m^3$ to about -4.0 $\mu g/m^3$ compared to the observations. At the same time, an overestimation during cold westerly wind conditions is apparent by now of up to 10.0 $\mu g/m^3$ with respect to the observations. Regarding warm westerly conditions a mean overestimation of about 4.0 $\mu g/m^3$ system can be recognized applying the multi-layering concept compared to the UBA measurements. Increased PM mass concentration levels are predominant in the whole model domain when using the multi-level model version (Tab. 4 and Fig. 7). In particular, the rural background concentration levels are increased by up to 8.4 $\mu g/m^3$ on average compared to the mixed layer approach. This leads to an average overestimation of rural background concentrations of up to 4.3 $\mu g/m^3$. The urban concentration levels are overestimated by up to 3.5 $\mu g/m^3$. The urban increment is about 4,9 $\mu g/m^3$ but is only slightly underestimated compared to the UBA measurements.

3.2.3 Model Performance

Model statistics show high agreement of the model simulations compared with observations (Tab. 4). An overall good representation of the observations can be achieved, with highest model performance evident for the multi-level version of the LOTOS-EUROS CTM. On average, high-resolution model simulations of the LOTOS-EUROS CTM show the best spatial performance with spatial and temporal correlation increasing with higher vertical model resolution. Best agreements can be observed for the dynamical downscaling approach of the COSMO-CLM input data combined with increased vertical resolution of the LOTOS-EUROS CTM, with spatial averaged model statistics of about 0.74 for the temporal correlation, 0.70 for the spatial correlation, -0.11 for the fractional bias, 0.23 for the normalized mean square error, 1.29 for the geometric variance and 0.91 for the geometric mean bias.

3.2.4 Composition of PM

In the following section, the comparison of the observed and modelled PM concentration is extended by chemical compounds (Fig. 9 and Fig. 10). This provides more information on the mechanisms causing to different results in the applied model configurations. The modelled and observed data were spatially averaged over the entire investigation area.

539

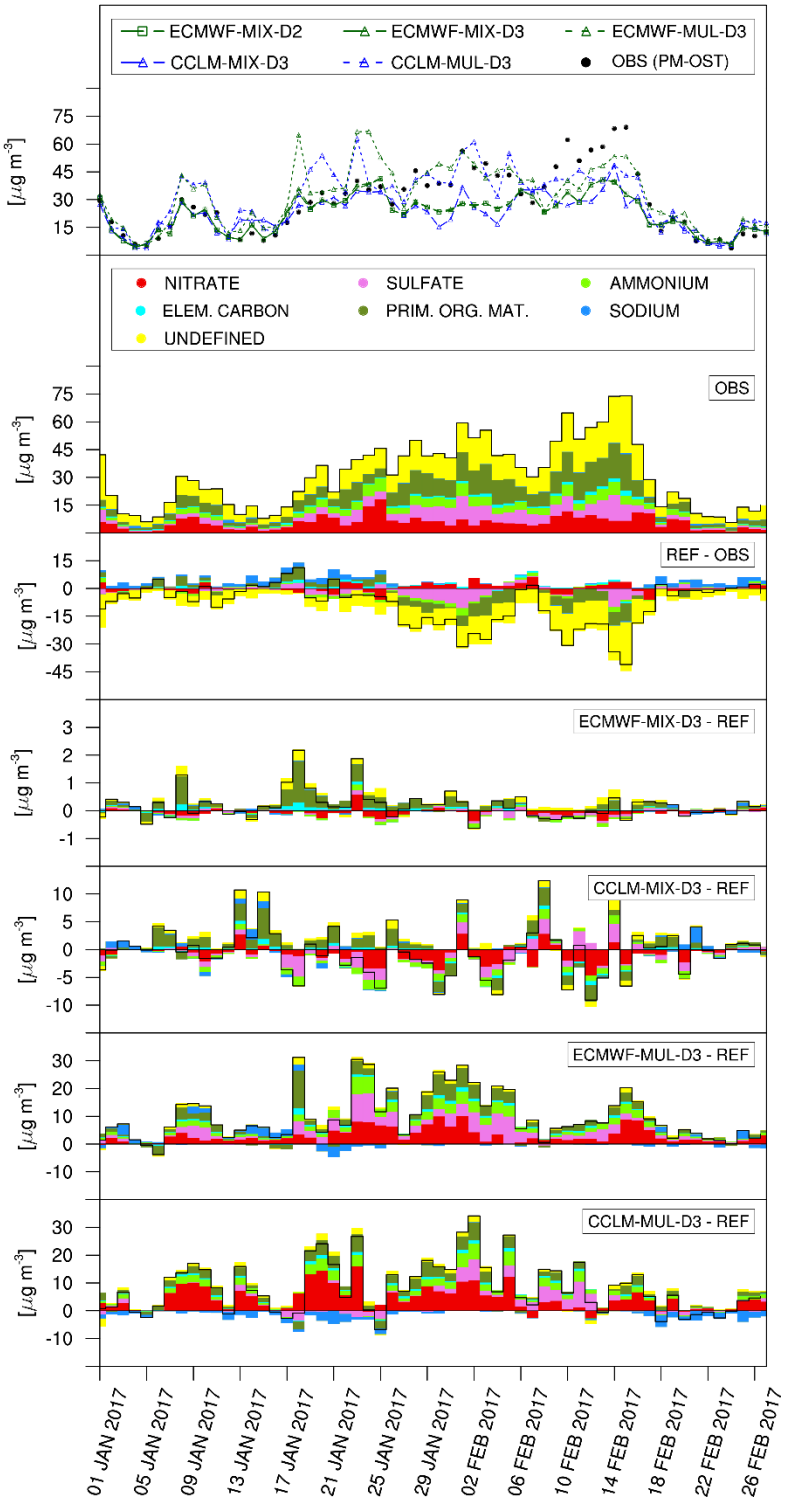

Fig. 9 Time series of observed (PM-OST) and modelled PM mass concentration levels (on top) for January to February 2017. Difference (black line) to the Observation (PM-OST) and the reference model (ECMWF-MIX-D2) are listed below and separated into their chemical composition (bar charts).

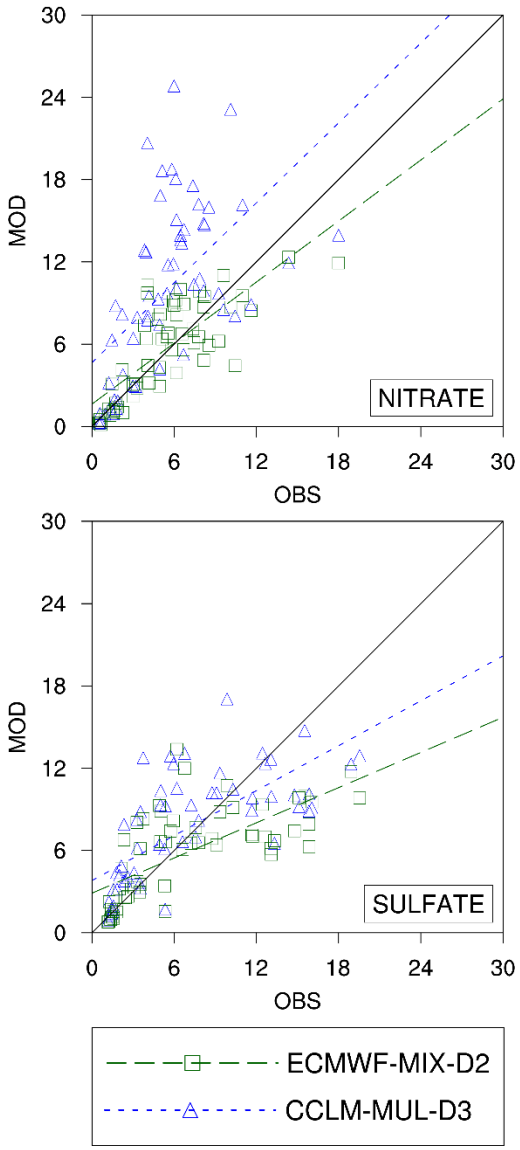

Fig. 10 Scatter plot of modelled (MOD) compared to of observed (OBS: PM-OST) mass concentration levels of nitrate (on top) and sulfate (bottom) for January to February 2017.

The observed PM composition shows high levels of nitrate (18 %), ammonium (10 %) and sulfate (13 %) as well as organic matter (23 %) for January to February 2017. Lower contributions can be attributed to sodium (1 %) and elemental carbon (3 %). The predominant compound is classified as undefined (34 %) which includes mineral dust, oxides, and other trace materials.

As mentioned in the previous section model simulations of the mixed-layer version indicate an overall underestimation of the total PM mass concentration especially during PM episodes in comparison to the observations. The largest part of the model bias can be attributed to an underestimation of sulfate, primary organic matter (POM), and the undefined fraction with estimated average underestimations ranging between -1.2 $\mu g/m^3$ for Sulfate and POM and of -8.0 $\mu g/m^3$ for the undefined fraction, respectively. By contrast, the components sodium, and elemental carbon show positive biases up to 1.4 $\mu g/m^3$ compared to the observations. Ammonium is slightly underestimated, whereas nitrate shows a small overestimation of (both about ± 0.2 $\mu g/m^3$).

Simulations by using different model resolutions in the horizontal or the vertical grid structure and different meteorological input data, especially affects individual chemical components as e.g. nitrate, and sulfate, which are highly sensitive compounds in the used model systems (Fig. 10). These observed sensitivities and their related overestimation of PM concentration levels compared to observations are primarily induced by the multi-level version of the LOTOS-EUROS CTM. The largest gain in mass concentration in the order of about 4.5 $\mu g/m^3$ is evident for nitrate, leading to an averaged overestimation of the same order of magnitude compared to the observations. Similar results are obvious for ammonium, which results in an overestimation of the averaged fraction of about 1.3 $\mu g/m^3$ compared to the measurements. Ammonium nitrate is a semi-volatile component and its formation depends a combination of factors including temperature, relative humidity, stability, and the precursor concentrations. In this case, the absence of the meteorological impact on ammonia emissions may increase the effects as the rise of ammonium nitrate occurs at (colder) moments when ammonia emissions are below average. The mass concentration of POM is increasing with higher vertical layering also by about 0.6 $\mu g/m^3$. By contrast, the sodium mass concentration was reduced and leads to a reduction of the model bias (0.2 $\mu g/m^3$). In all simulations a below average performance is found for the formation of sulfate. Compared to the observations, the model bias (-0.4 $\mu g/m^3$) for sulfate is considerably reduced on average, but still the temporal trend is difficult to capture.

Using different meteorological input data is not as large reflected in the distribution of the chemical compounds. The results differ in the concentration mass corresponding to the conclusions mentioned above with small changes in the model bias of nitrate and POM ranging within 0.5 $\mu g/m^3$ when using the COSMO-CLM model. By contrast, the fraction of sulfate is changed for

January to February 2017 and counteracts the model bias. In comparison to the ECMWF driven model system, a negative difference prior to and a positive one during the PM episode appears.

The smallest variations in the component distribution can be observed by increasing the model resolution using the zooming approach in the LOTOS-EUROS CTM, with higher POM concentration and lower nitrate levels modelled for the observation sites for January to February 2017. Averaged differences of up to 0.3 $\mu g/m^3$ with respect to the lower resolution can be recognized. The impact of elemental carbon becomes more relevant with higher resolution increasing the mass concentration in the order of 0.1 $\mu g/m^3$, which results in a larger overestimation of about 0.4 $\mu g/m^3$ compared to the observation.

4 Discussion and Conclusions

We successfully developed an interface to the COSMO-CLM model and explored the impact of different meteorological input data and horizontal and vertical resolutions for the LOTOS-EUROS CTM. The quality of the meteorological input data are a major impact factor on chemical transport modelling and can thus be one reason for excessive mixing (Vautard et al. (2012)). Our study shows that meteorological conditions can significantly be improved by applying the dynamical downscaling approach of the COSMO-CLM model compared to the ECMWF reference data. Especially the comparison to observed MLHs, derived from radiosonde data using the bulk Richardson method (Seibert et al., 2000), exhibits a good agreement. Weaknesses are apparent representing the MLH top with a low bias, while the temporal evolution and the variability are well reflected. Previous studies also mentioned a systematic underestimation of the PBL height of the COSMO model during convective situations or frontal crossings, comparable to the prevailing conditions during the selected investigation period (Fay & Neunhäuserer, 2005). Baars et al. (2008) also published model simulation results of the COSMO model indicating a too low MLH of about 20%. In the study of Baars et al. (2008) the dependency to cloud cover was emphasized with highest underestimation appearing when clouds are predicted by the model but are not existent at all. By contrast, the study by Collaud Coen et al. (2014) indicates a general overestimation of the COSMO model caused by a too rapid increase in the early morning hours, with larger differences during cloudy conditions as well. As reason of these positive and negative model bias compared to the observations, differences in the stratification of

atmospheric parameters can be regarded as the main impact factor, caused in particular by the orographic situation in the studies mentioned above.

To provide reliable meteorological conditions of the PBL for the investigation area of Berlin, we attempted to improve the variability of the MLH by using different PBL parameterizations of the COSMO-CLM model. Neither the simulation of the mean nor the representation of the variability can be improved much by the sensitivity simulations of the COSMO-CLM model. The overall total variation caused by the parameterizations is small and no clear bias correction can be achieved. Previous studies already mentioned similar difficulties adopting parametrizations. Buzzi et al. (2011) for instance indicates a loss of information of the near-surface temperature inversion when too low diffusion coefficients are applied, with high values are required to avoid low mixing. A further study by Meissner et al. (2009) indicates minor impact of varying physical model parameters compared to changing meteorological driving data of the COSMO-CLM model. This may indicate that the downscaling domain of COSMO should be increased substantially in the future to widen the ensemble spread.

In fact, the MLH is not a physical parameter, it is simply a diagnostic quantity and cannot be directly measured with the determination associated with certain limitations (Schäfer et al., 2006). However, studies on the comparability of MLH retrievals deliver significant differences especially depending on the meteorological conditions. Based on the algorithm used to derive the MLH, such as temperature profiles, sodar results and lidar, various solutions can be obtained (Coulter, 1979; Seidel et al., 2010; Haeffelin et al., 2012; Beyrich & Leps, 2012). The differences even increase when complex methods are used to distinguish between several PBL types (Collaud Coen et al., 2014). This leads to a validation and implementation problem in CTMs. To avoid the issue of the derivation problem, we advise not to use the MLH as input or validation data for CTMs in contrast to previous recommendations by studies like as Geiß et al. (2017). In accordance with the suggestion of Hanna & Yang (2001) we therefore increased the vertical grid resolution of the model to better reflect shallow inversion conditions by applying the recent multi-layering version of the LOTOS-EUROS CTM.

The impact on the PM mass concentration of the vertical layering in the LOTOS-EUROS CTM is much larger than the planetary boundary layer meteorology, with the multi-level approach of the LOTOS-EUROS CTM significantly increasing the concentration mass in the investigation

area of Berlin. Major impact can be associated to cold stagnant weather conditions, especially easterly wind periods and a better representation of high transboundary PM contributions. By contrast, warm periods are not as large modified by using the high vertical grid structure. This can be attributed to a modified distribution of the chemical compounds, especially nitrate, and ammonium, which responded highly sensitive within the used model set-ups. Compared to the mixed-layer version the nitrate and ammonium concentration levels are increased and lead to an increased total PM mass concentration when applying the higher resolved vertical layering structure.

This study and recent assessment for NO_2 and ozone show that the multi-level approach of the LOTOS-EUROS CTM keeps the pollutants closer to the surface than the mixed layer approach (Escudero et al. (2019); Fallah et al (2020)). Fallah et. al. (2020) further reveals a seasonal relationship of the nitrogen oxide mass concentration levels dependent on the applied vertical set-up, with an overestimated mixing in the mixed-layer version of the LOTOS-EUROS CTM. The similarity of the results for summer was large, where a better performance for the multi-level model version was found for the winter season compared to the mixed-layer approach. However, the refined vertical layering still results in too high PM concentration levels in urban areas and non-polluted periods, thus further investigations of the model set-up must be carried out.

Higher resolved model simulations and the use of the COSMO-CLM model as meteorological input data, leads to a more realistic representation of the urban-increment compared to coarser model simulations driven by the EMCWF model. Especially the spatial distribution of the PM background concentration is considerably improved. The higher horizontal resolution of the LOTOS-EUROS-CTM in combination with high resolution meteorological input data hence leads to less artificial dilution in urban areas.

Individual chemical compounds should be examined and considered separately by applying a labelling approach. Underestimated processes like as resuspension due to traffic, construction or agriculture could then easily be identified to improve the emission inventory for the Berlin agglomeration. Further investigations based on source apportionment and receptor studies and their comparison to PMF observations should be carried out to further enhance the insight of long-range and local contributions in the investigation area of Berlin.

Acknowledgment

The work presented here was funded through the German Environment Agency (UBA), Dessau-Roßlau, Project number: FKZ 3716 51 203 0. The authors gratefully acknowledge the provision of data in the project “PM-Ost” from the Berlin Senate Department for the Environment, Transport and Climate Protection, Berlin, the Saxon State Office for Environment, Agriculture and Geology (LfULG), Dresden-Pillnitz, the State Office for Environment (LfU) of the Federal State of Brandenburg, Potsdam, and the State Office for Environment, Nature and Geology (LUNG) of the Federal State of Mecklenburg-Western Pomerania, Güstrow.

References

ARAKAWA, A., & LAMB, V. R. (1977). Computational Design of the Basic Dynamical Processes of the UCLA General Circulation Model. In J. CHANG (Ed.), *General Circulation Models of the Atmosphere* (Vol. 17, pp. 173–265). Elsevier. https://doi.org/https://doi.org/10.1016/B978-0-12-460817-7.50009-4

Baars, H., Ansmann, A., Engelmann, R., & Althausen, D. (2008). Continuous monitoring of the boundary-layer top with lidar. *Atmospheric Chemistry and Physics*, *8*(23), 7281–7296. https://doi.org/10.5194/acp-8-7281-2008

Banks, R. F., & Baldasano, J. M. (2016). Impact of WRF model PBL schemes on air quality simulations over Catalonia, Spain. *Science of the Total Environment*, *572*, 98–113. https://doi.org/10.1016/j.scitotenv.2016.07.167

Banzhaf, S., Schaap, M., Kerschbaumer, A., Reimer, E., Stern, R., Van Der Swaluw, E., & Builtjes, P. (2012). Implementation and evaluation of pH-dependent cloud chemistry and wetdeposition in the chemical transport model REM-Calgrid. *Atmospheric Environment*. https://doi.org/10.1016/j.atmosenv.2011.10.069

Beekmann, M., Prévôt, A. S. H., Drewnick, F., Sciare, J., Pandis, S. N., Denier Van Der Gon, H. A. C., et al. (2015). In situ, satellite measurement and model evidence on the dominant regional contribution to fine particulate matter levels in the Paris megacity. *Atmospheric Chemistry and Physics*, *15*(16), 9577–9591. https://doi.org/10.5194/acp-15-9577-2015

Belis, C. A., Pernigotti, D., Pirovano, G., Favez, O., Jaffrezo, J. L., Kuenen, J., et al. (2020).

693 Evaluation of receptor and chemical transport models for PM10 source apportionment.
694 *Atmospheric Environment: X*, *5*, 100053. https://doi.org/10.1016/J.AEAOA.2019.100053

695 Beyrich, F., & Leps, J. P. (2012). An operational mixing height data set from routine
696 radiosoundings at Lindenberg: Methodology. *Meteorologische Zeitschrift*, *21*(4), 337–348.
697 https://doi.org/10.1127/0941-2948/2012/0333

698 Boldo, E., Medina, S., LeTertre, A., Hurley, F., Mücke, H. G., Ballester, F., et al. (2006).
699 Apheis: Health impact assessment of long-term exposure to PM2.5 in 23 European cities.
700 *European Journal of Epidemiology*, *21*(6), 449–458. https://doi.org/10.1007/s10654-006-
701 9014-0

702 Brook, R. D., Rajagopalan, S., Pope, C. A., Brook, J. R., Bhatnagar, A., Diez-Roux, A. V., et al.
703 (2010, June 1). Particulate matter air pollution and cardiovascular disease: An update to the
704 scientific statement from the american heart association. *Circulation*.
705 https://doi.org/10.1161/CIR.0b013e3181dbece1

706 Brüggemann, E., Gerwig, H., Gnauk, T., Müller, K., & Herrmann, H. (2009). Influence of
707 seasons, air mass origin and day of the week on size-segregated chemical composition of
708 aerosol particles at a kerbside. *Atmospheric Environment*, *43*(15), 2456–2463.
709 https://doi.org/10.1016/J.ATMOSENV.2009.01.054

710 Businger, J. A., Wyngaard, J. C., Izumi, Y., & Bradley, E. F. (1971). Flux-Profile Relationships
711 in the Atmospheric Surface Layer. *Journal of the Atmospheric Sciences*, *28*(2), 181–189.
712 https://doi.org/10.1175/1520-0469(1971)028<0181:fprita>2.0.co;2

713 Buzzi, M., Rotach, M. W., Holtslag, M., & Holtslag, A. A. M. (2011). Evaluation of the
714 COSMO-SC turbulence scheme in a shear-driven stable boundary layer. *Meteorologische*
715 *Zeitschrift*, *20*(3), 335–350. https://doi.org/10.1127/0941-2948/2011/0050

716 Chang, J. C., & Hanna, S. R. (2004). Air quality model performance evaluation. *Meteorology*
717 *and Atmospheric Physics*, *87*(1–3), 167–196. https://doi.org/10.1007/s00703-003-0070-7

718 Collaud Coen, M., Praz, C., Haefele, A., Ruffieux, D., Kaufmann, P., & Calpini, B. (2014).
719 Determination and climatology of the planetary boundary layer height above the Swiss
720 plateau by in situ and remote sensing measurements as well as by the COSMO-2 model.
721 *Atmospheric Chemistry and Physics*, *14*(23), 13205–13221. https://doi.org/10.5194/acp-14-

13205-2014

Costa, S., Ferreira, J., Silveira, C., Costa, C., Lopes, D., Relvas, H., et al. (2014, August 18). Integrating health on air quality assessment - Review report on health risks of two major european outdoor air pollutants: PM and NO2. *Journal of Toxicology and Environmental Health - Part B: Critical Reviews*. Taylor & Francis. https://doi.org/10.1080/10937404.2014.946164

Coulter, R. L. (1979). A Comparison of Three Methods for Measuring Mixing-Layer Height. *Journal of Applied Meteorology*, *18*(11), 1495–1499. https://doi.org/10.1175/1520-0450(1979)018<1495:ACOTMF>2.0.CO;2

Dee, D. P., Uppala, S. M., Simmons, A. J., Berrisford, P., Poli, P., Kobayashi, S., et al. (2011). The ERA-Interim reanalysis: configuration and performance of the data assimilation system. *Quarterly Journal of the Royal Meteorological Society*, *137*(656), 553–597. https://doi.org/10.1002/qj.828

Doms, G., & Baldauf, M. (2018). *A Description of the Nonhydrostatic Regional COSMO-Model Part I: Dynamics and Numerics - COSMO-Model 5.5* (http://www.cosmo-model.org/content/model/documentation/core/cosmoDyncsNumcs.pdf). P.O. Box 100465, 63004 Offenbach, Germany.

Doms, G., Förstner, J., Heise, E., Herzog, H.-J., Mironov, D., Raschendorfer, M., et al. (2011). *A Description of the Nonhydrostatic Regional COSMO-Model Part II: Physical Parameterization - LM_F90 4.20* (http://www.cosmo-model.org/content/model/documentation/core/cosmoPhysParamtr.pdf). P.O. Box 100465, 63004 Offenbach, Germany.

Eckermann, S. (2009). Hybrid σ-p coordinate choices for a global model. *Monthly Weather Review*, *137*(1), 224–245. https://doi.org/10.1175/2008MWR2537.1

EEA. (2018). Air quality in Europe - 2018 report. *European Environment Agency (EEA) Report No 12/2018*. Retrieved from https://www.eea.europa.eu/publications/air-quality-in-europe-2018

Engler, C., Birmili, W., Spindler, G., & Wiedensohler, A. (2012). Analysis of exceedances in the daily PM 10 mass concentration (50 μg m -3) at a roadside station in Leipzig, Germany.

Atmospheric Chemistry and Physics, *12*(21), 10107–10123. https://doi.org/10.5194/acp-12-10107-2012

Escudero, M., Segers, A., Kranenburg, R., Querol, X., Alastuey, A., Borge, R., et al. (2019). Analysis of summer O3 in the Madrid air basin with the LOTOS-EUROS chemical transport model. *Atmospheric Chemistry and Physics Discussions*, 1–40. https://doi.org/10.5194/acp-2019-334

European Parliament; European Council. (2008). Directive 2008/50/EC on ambient air quality and cleaner air for Europe. *Official Journal of the European Communities*, *152*, 1–43. https://doi.org/http://eur-lex.europa.eu/LexUriServ/LexUriServ.do?uri=OJ:L:2008:152:0001:0044:EN:PDF

Fay, B., & Neunhäuserer, L. (2005). Evaluation of very high-resolution simulations with the non-hydrostatic numerical weather prediction model Lokalmodell for urban air pollution episodes in Helsinki, Oslo and Valencia. *Atmospheric Chemistry and Physics Discussions*, *5*. https://doi.org/10.5194/acpd-5-8233-2005

Flemming, J., Inness, A., Flentje, H., Huijnen, V., Moinat, P., Schultz, M. G., & Stein, O. (2009). Coupling global chemistry transport models to ECMWF's integrated forecast system. *Geoscientific Model Development*, *2*(2), 253–265. https://doi.org/10.5194/gmd-2-253-2009

Fountoukis, C., & Nenes, A. (2007). ISORROPIA II: a computationally efficient thermodynamic equilibrium model for K^+–Ca^{2+}–Mg^{2+}–NH_4^+–Na^+–$SO_4^{2\−}$–NO_3<sup>. *Atmos. Chem. Phys.*, *7*(17), 4639–4659. Retrieved from https://www.atmos-chem-phys.net/7/4639/2007/

Garg, S., & Sinha, B. (2017). Determining the contribution of long-range transport, regional and local source areas, to PM10 mass loading in Hessen, Germany using a novel multi-receptor based statistical approach. *Atmospheric Environment*, *167*, 566–575. https://doi.org/10.1016/j.atmosenv.2017.08.029

Geiß, A., Wiegner, M., Bonn, B., Schäfer, K., Forkel, R., Von Schneidemesser, E., et al. (2017). Mixing layer height as an indicator for urban air quality? *Atmospheric Measurement Techniques*, *10*(8), 2969–2988. https://doi.org/10.5194/amt-10-2969-2017

van der Gon, H. A. C., Bergström, R., Fountoukis, C., Johansson, C., Pandis, S. N., Simpson, D., & Visschedijk, A. J. H. (2015). Particulate emissions from residential wood combustion in Europe – revised estimates and an evaluation. *Atmospheric Chemistry and Physics*, *15*(11), 6503–6519. https://doi.org/10.5194/acp-15-6503-2015

Haeffelin, M., Angelini, F., Morille, Y., Martucci, G., Frey, S., Gobbi, G. P., et al. (2012). Evaluation of Mixing-Height Retrievals from Automatic Profiling Lidars and Ceilometers in View of Future Integrated Networks in Europe. *Boundary-Layer Meteorology*, *143*(1), 49–75. https://doi.org/10.1007/s10546-011-9643-z

Hanna, S. R., & Yang, R. (2001). Evaluations of mesoscale models' simulations of near-surface winds, temperature gradients, and mixing depths. *Journal of Applied Meteorology*, *40*(6), 1095–1104. https://doi.org/10.1175/1520-0450(2001)040<1095:EOMMSO>2.0.CO;2

Hendriks, C., Kranenburg, R., Kuenen, J., van Gijlswijk, R., Wichink Kruit, R., Segers, A., et al. (2013). The origin of ambient particulate matter concentrations in the Netherlands. *Atmospheric Environment*. https://doi.org/10.1016/j.atmosenv.2012.12.017

Herzog, H.-J., Schubert, U., Vogel, G., Fiedler, A., & Kirchner, R, . (2002). LLM- the high-resolving nonhydrostatic simulation model in the DWD-project LITFASS.Part I: Modelling technique and simulation method. *Technical Report No. 4*. Retrieved from https://www.dwd.de/SharedDocs/downloads/DE/modelldokumentationen/nwv/veroeffentlichungen/Cosmo_tech_rep/costr4.pdf?__blob=publicationFile&v=2

Herzog, H.-J., Vogel, G., & Schubert, U. (2002). LLM - a nonhydrostatic model applied to high-resolving simulations of turbulent fluxes over heterogeneous terrain. *Theoretical and Applied Climatology*, *73*(1–2), 67–86. https://doi.org/10.1007/s00704-002-0694-4

Hu, X. M., Nielsen-Gammon, J. W., & Zhang, F. (2010). Evaluation of three planetary boundary layer schemes in the WRF model. *Journal of Applied Meteorology and Climatology*, *49*(9), 1831–1844. https://doi.org/10.1175/2010JAMC2432.1

Kaiser, J. W., Heil, A., Andreae, M. O., Benedetti, A., Chubarova, N., Jones, L., et al. (2012). Biomass burning emissions estimated with a global fire assimilation system based on observed fire radiative power. *Biogeosciences*, *9*(1), 527–554. https://doi.org/10.5194/bg-9-527-2012

Kranenburg, R., Segers, A. J., Hendriks, C., & Schaap, M. (2013). Source apportionment using LOTOS-EUROS: module description and evaluation. *Geoscientific Model Development*, *6*(3), 721–733. https://doi.org/10.5194/gmd-6-721-2013

Lenschow, P., Abraham, H. J., Kutzner, K., Lutz, M., Preuß, J. D., & Reichenbächer, W. (2001). Some ideas about the sources of PM10. *Atmospheric Environment*, *35*(SUPPL. 1). https://doi.org/10.1016/s1352-2310(01)00122-4

LFU. (2018). *Luftqualität in Brandenburg Jahresbericht 2018*. Potsdam. Retrieved from https://lfu.brandenburg.de/cms/media.php/lbm1.a.3310.de/Luftqualitaet_BB_2018.pdf

Lim, S. S., Vos, T., Flaxman, A. D., Danaei, G., Shibuya, K., Adair-Rohani, H., et al. (2012). A comparative risk assessment of burden of disease and injury attributable to 67 risk factors and risk factor clusters in 21 regions, 1990-2010: A systematic analysis for the Global Burden of Disease Study 2010. *The Lancet*, *380*(9859), 2224–2260. https://doi.org/10.1016/S0140-6736(12)61766-8

Louis, J.-F. (1979). A parametric model of vertical eddy fluxes in the atmosphere. *Boundary-Layer Meteorology*, *17*(2), 187–202. https://doi.org/10.1007/BF00117978

Manders, A. M. M., Builtjes, P. J. H., Curier, L., van der Gon, H. A. C., Hendriks, C., Jonkers, S., et al. (2017). Curriculum vitae of the LOTOS--EUROS (v2.0) chemistry transport model. *Geoscientific Model Development*, *10*(11), 4145–4173. https://doi.org/10.5194/gmd-10-4145-2017

Marécal, V., Peuch, V.-H., Andersson, C., Andersson, S., Arteta, J., Beekmann, M., et al. (2015). A regional air quality forecasting system over Europe: the MACC-II daily ensemble production. *Geoscientific Model Development*, *8*(9), 2777–2813. https://doi.org/10.5194/gmd-8-2777-2015

Meissner, C. S., Panitz, H.-J. F., & Kottmeier, C. (2009). High-resolution sensitivity studies with the regional climate model COSMO-CLM. *Meteorologische Zeitschrift*, *18*(5), 543–557. https://doi.org/10.1127/0941-2948/2009/0400

Mellor, G. L., & Yamada, T. (1974). A Hierarchy of Turbulence Closure Models for Planetary Boundary Layers. *Journal of the Atmospheric Sciences*, *31*(7), 1791–1806. https://doi.org/10.1175/1520-0469(1974)031<1791:AHOTCM>2.0.CO;2

Mues, A., Manders, A., Schaap, M., Kerschbaumer, A., Stern, R., & Builtjes, P. (2012). Impact of the extreme meteorological conditions during the summer 2003 in Europe on particulate matter concentrations. *Atmospheric Environment*, *55*, 377–391. https://doi.org/10.1016/j.atmosenv.2012.03.002

Mues, A., Kuenen, J., Hendriks, C., Manders, A., Segers, A., Scholz, Y., et al. (2014). Sensitivity of air pollution simulations with LOTOS-EUROS to the temporal distribution of anthropogenic emissions. *Atmospheric Chemistry and Physics*, *14*(2), 939–955. https://doi.org/10.5194/acp-14-939-2014

Muller, E. (1981). Turbulent flux parameterization in a regional-scale model. In *Workshop on Planetary Boundary Layer parameterization, 25-27 November 1981* (pp. 193–220). Shinfield Park, Reading: ECMWF. Retrieved from https://www.ecmwf.int/node/11313

van Pinxteren, D., Mothes, F., Spindler, G., Fomba, K. W., & Herrmann, H. (2019). Trans-boundary PM10: Quantifying impact and sources during winter 2016/17 in eastern Germany. *Atmospheric Environment*, *200*, 119–130. https://doi.org/10.1016/j.atmosenv.2018.11.061

Potier, E., Waked, A., Bourin, A., Minvielle, F., Péré, J. C., Perdrix, E., et al. (2019). Characterizing the regional contribution to PM10 pollution over northern France using two complementary approaches: Chemistry transport and trajectory-based receptor models. *Atmospheric Research*, *223*, 1–14. https://doi.org/https://doi.org/10.1016/j.atmosres.2019.03.002

Rockel, B., Will, A., & Hense, A. (2008). The Regional Climate Model COSMO-CLM (CCLM). *Meteorologische Zeitschrift*, *17*(4), 347–348. https://doi.org/10.1127/0941-2948/2008/0309

Schaap, M., van Loon, M., ten Brink, H. M., Dentener, F. J., & Builtjes, P. J. H. (2004). Secondary inorganic aerosol simulations for Europe with special attention to nitrate. *Atmospheric Chemistry and Physics*, *4*(3), 857–874. https://doi.org/10.5194/acp-4-857-2004

Schäfer, K., Emeis, S., Hoffmann, H., & Jahn, C. (2006). Influence of mixing layer height upon air pollution in urban and sub-urban areas. *Meteorologische Zeitschrift*, *15*(6), 647–658. https://doi.org/10.1127/0941-2948/2006/0164

Schättler, U., Doms, G., & Schraff, C. (2019). *A Description of the Nonhydrostatic Regional*

COSMO-Model Part VII: User's Guide. P.O. Box 100465, 63004 Offenbach, Germany.

Schneider, C., Pelzer, M., Toenges-Schuller, N., Nacken, M., & Niederau, A. (2016). ArcGIS basierte Lösung zur detaillierten, deutschlandweiten Verteilung (Gridding) nationaler Emissionsjahreswerte auf Basis des Inventars zur Emissionsberichterstattung - Kurzfassung ; UBA TEXTE 71/2016. *Für Mensch & Umwelt*. Retrieved from http://www.umweltbundesamt.de/publikationen

Seibert, P., Beyrich, F., Gryning, S. E., Joffre, S., Rasmussen, A., & Tercier, P. (2000). Review and intercomparison of operational methods for the determination of the mixing height. *Atmospheric Environment*. https://doi.org/10.1016/S1352-2310(99)00349-0

Seidel, D. J., Ao, C. O., & Li, K. (2010). Estimating climatological planetary boundary layer heights from radiosonde observations: Comparison of methods and uncertainty analysis. *Journal of Geophysical Research: Atmospheres*, *115*(D16). https://doi.org/10.1029/2009JD013680

SenStadt. (2019). *Luftreinhalteplan für Berlin 2. Fortschreibung (Air pollution management plan Berlin 2. Update)* (Berlin: lebenswerter). Berlin. Retrieved from https://www.berlin.de/senuvk/umwelt/luft/luftreinhaltung/luftreinhalteplan_2025/download/Luftreinhalteplan.pdf

Spindler, G., Müller, K., Brüggemann, E., Gnauk, T., & Herrmann, H. (2004). Long-term size-segregated characterization of PM 10, PM 2.5, and PM 1 at the IfT research station Melpitz downwind of Leipzig (Germany) using high and low-volume filter samplers. In *Atmospheric Environment* (Vol. 38, pp. 5333–5347). https://doi.org/10.1016/j.atmosenv.2003.12.047

Stern, R., Builtjes, P., Schaap, M., Timmermans, R., Vautard, R., Hodzic, A., et al. (2008). A model inter-comparison study focussing on episodes with elevated PM10 concentrations. *Atmospheric Environment*, *42*(19), 4567–4588. https://doi.org/https://doi.org/10.1016/j.atmosenv.2008.01.068

Stull, R. B. (1988). *An Introduction to Boundary Layer Meteorology.* Dordrecht, Boston and London, 666 p.: Kluwer Academic Publishers. https://doi.org/http://dx.doi.org/10.1007/978-94-009-3027-8

Tai, A. P. K., Mickley, L. J., & Jacob, D. J. (2010). Correlations between fine particulate matter (PM2.5) and meteorological variables in the United States: Implications for the sensitivity of PM2.5 to climate change. *Atmospheric Environment*. https://doi.org/10.1016/j.atmosenv.2010.06.060

Thunis, P., Degraeuwe, B., Pisoni, E., Trombetti, M., Peduzzi, E., Belis, C. A., et al. (2018). PM2.5 source allocation in European cities: A SHERPA modelling study. *Atmospheric Environment*, *187*, 93–106. https://doi.org/10.1016/J.ATMOSENV.2018.05.062

Timmermans, R., Kranenburg, R., Manders, A., Hendriks, C., Segers, A., Dammers, E., et al. (2017). Source apportionment of PM2.5 across China using LOTOS-EUROS. *Atmospheric Environment*. https://doi.org/10.1016/j.atmosenv.2017.06.003

Timmermans, R., Kranenburg, R., Hendriks, C., Thürkow, M., Kirchner, I., van Pinxteren, D., & Schaap, M. (2020). Establishing the Origin of Particulate Matter in Eastern Germany Using an Improved Regional Modelling Framework (pp. 3–8). https://doi.org/10.1007/978-3-030-22055-6_1

UBA. (2019). *Luftqualität 2018*. *Für Mensch & Umwelt*. Retrieved from www.umweltbundesamt.de/publikationen/

Vautard, R., Moran, M. D., Solazzo, E., Gilliam, R. C., Matthias, V., Bianconi, R., et al. (2012). Evaluation of the meteorological forcing used for the Air Quality Model Evaluation International Initiative (AQMEII) air quality simulations. *Atmospheric Environment*. https://doi.org/10.1016/j.atmosenv.2011.10.065

Vogelezang, D. H. P., & Holtslag, A. A. M. (1996). Evaluation and model impacts of alternative boundary-layer height formulations. *Boundary-Layer Meteorology*, *81*(3), 245–269. https://doi.org/10.1007/BF02430331

Walcek, C. J. (2000). Minor flux adjustment near mixing ratio extremes for simplified yet highly accurate monotonic calculation of tracer advection. *Journal of Geophysical Research: Atmospheres*, *105*(D7), 9335–9348. https://doi.org/10.1029/1999JD901142

Wetzel, P. J. (1982). Toward Parameterization of the Stable Boundary Layer. *Journal of Applied Meteorology*, *21*(1), 7–13. https://doi.org/10.1175/1520-0450(1982)021<0007:TPOTSB>2.0.CO;2

Whitten, G. Z., Hogo, H., & Killus, J. P. (1980). The carbon-bond mechanism: a condensed kinetic mechanism for photochemical smog. *Environ. Sci. Technol.*, *14*(6), 690–700. https://doi.org/10.1021/es60166a008

Wichink Kruit, R. J., Schaap, M., Sauter, F. J., van Zanten, M. C., & van Pul, W. A. J. (2012). Modeling the distribution of ammonia across Europe including bi-directional surface–atmosphere exchange. *Biogeosciences*, *9*(12), 5261–5277. https://doi.org/10.5194/bg-9-5261-2012

World Health Organization, W. (2005). *WHO Air quality guidelines for particulate matter, ozone, nitrogen dioxide and sulfur dioxide: Global update 2005*. *WHO*. https://doi.org/10.1016/0004-6981(88)90109-6

Van Zanten, M. C., Sauter, F. J., Wichink Kruit, R. J., Van Jaarsveld, J. A., & Van Pul, W. A. J. (2010). *Description of the DEPAC module: Dry deposition modelling with DEPAC_GCN2010 ; Report 680180001/2010*. RIVM, P.O. Box 1, 3720 BA Bilthoven, the Netherlands Tel +31 30 274 91 11 www.rivm.nl. Retrieved from https://www.rivm.nl/bibliotheek/rapporten/680180001.pdf

Zhang, H., Wang, Y., Hu, J., Ying, Q., & Hu, X. M. (2015). Relationships between meteorological parameters and criteria air pollutants in three megacities in China. *Environmental Research*, *140*, 242–254. https://doi.org/10.1016/j.envres.2015.04.004

Zhang, L., Gong, S., Padro, J., & Barrie, L. (2001). A size-segregated particle dry deposition scheme for an atmospheric aerosol module. *Atmospheric Environment*, *35*(3), 549–560. https://doi.org/https://doi.org/10.1016/S1352-2310(00)00326-5